



ARTICLE

Initiation of Parkinson's disease from gut to brain by δ -secretase

Eun Hee Ahn¹, Seong Su Kang¹, Xia Liu¹, Guiqin Chen², Zhentao Zhang², Bindu Chandrasekharan¹, Ashfaqul M. Alam¹, Andrew S. Neish¹, Xuebing Cao³ and Keqiang Ye¹

Lewy pathology, composed of α -Synuclein (α -Syn) inclusions, a hallmark of Parkinson's disease (PD), progressively spreads from the enteric nervous system (ENS) to the central nervous system (CNS). However, it remains unclear how this process is regulated at a molecular level. Here we show that δ -secretase (asparagine endopeptidase, AEP) cleaves both α -Syn at N103 and Tau at N368, and mediates their fibrillization and retrograde propagation from the gut to the brain, triggering nigra dopaminergic neuronal loss associated with Lewy bodies and motor dysfunction. α -Syn N103 and Tau N368 robustly interact with each other and are highly elevated in PD patients' gut and brain. Chronic oral administration of the neurotoxin rotenone induces AEP activation and α -Syn N103/Tau N368 complex formation in the gut, eliciting constipation and dopaminergic neuronal death in an AEP-dependent manner. Preformed fibrils (PFFs) of α -Syn N103/Tau N368 are more neurotoxic and compact, and aggregate more quickly along the vagus nerve than their FL/FL counterparts or the individual fragments' fibrils. Colonic injection of PFFs induces PD pathologies, motor dysfunctions, and cognitive impairments. Thus, δ -secretase plays a crucial role in initiating PD pathology progression from the ENS to the CNS.

Cell Research (2019) 0:1–18; <https://doi.org/10.1038/s41422-019-0241-9>

INTRODUCTION

Parkinson's disease (PD) is the second most common neurodegenerative disorder characterized by motor and non-motor symptoms. Its pathological hallmarks include loss of dopaminergic neurons of the substantia nigra (SN)-striatum system and presence of proteinaceous cytoplasmic inclusions, known as Lewy Bodies (LBs), in the remaining dopaminergic neurons.¹ PD etiology is incompletely understood, but is believed to be multifactorial involving both genetic and environmental interactions. The major component of the LB is aggregated α -Synuclein (α -Syn).² The LBs stain positively for α -Syn, ubiquitin, and α -Syn specifically phosphorylated on S129, which is mainly found in LBs and Lewy neurites, though minor portion of α -Syn p-S129 also exists in normal brain.³ A pathogenic role for α -Syn in PD is supported by various genetic data. For instance, multiplications of SNCA gene and various point mutations in this gene result in dominant familial parkinsonism,^{4–6} indicating that increased level of normal α -Syn protein is sufficient to cause the disease. Moreover, certain polymorphisms in SNCA are major risk factors for sporadic PD.⁷ The abnormal accumulation of α -Syn, resulting from an unbalanced production and/or degradation, triggers dopaminergic neuronal death in both familial and sporadic cases of PD.⁸

Tau-immunoreactive LBs are detected in the brain of sporadic PD and dementia with Lewy body (DLB) patients.^{9,10} Genome-wide association studies (GWAS) have confirmed polymorphisms in SNCA and Tau (MAPT) as common risk factors for PD.^{7,11} Interestingly, Tau and α -Syn interact with each other,¹² and recombinant α -Syn and Tau proteins synergistically promote the fibrillization of each other.¹³ Furthermore, α -Syn preformed fibrils

(PFFs) induced Tau aggregation in cultured non-neuronal cells and primary neurons.^{14,15} Recently, it has been reported that interactions between Tau and α -Syn augment neurotoxicity in a *Drosophila* model of PD. Interactions between α -Syn and Tau cause disruption of cytoskeletal organization, axonal transport defects and aberrant synaptic organization, contributing to neuronal dysfunction and death in a *Drosophila* model of PD.¹⁶

Many environmental risk factors have been implicated in PD pathogenesis. One of the primary classes of environmental agents associated with PD is pesticides.¹⁷ Several commercial pesticides inhibit complex I of the electron transport chain (ETC) in mitochondria,¹⁸ but their role in causing parkinsonism is unknown. One such pesticide is rotenone, which is a prototypical example of how exposure to an exogenous toxin can reproduce clinical and pathological features of PD in an animal model.^{19,20} Hydrophobic nature of rotenone facilitates easy translocation across the biological membranes, including the blood brain barrier, thereby gaining access to all organs quickly after exposure.²¹ In addition to selective nigrostriatal degeneration, the rotenone model accurately recapitulated many other features of human PD including anatomical, neurochemical, behavioral and neuropathological characteristics. Chronic rotenone exposure leads to the accumulation and aggregation of both α -Syn and ubiquitin, and caspase-activated cell death in neurons.^{22–24} Noticeably, it also triggers impairment of gastrointestinal (GI) motility,^{25,26} and accumulating evidence supports that Lewy pathology spreads from the GI tract to the brain.²⁷ Oral administration of rotenone (5 mg/kg), which does not enter the systemic circulation or inhibit mitochondrial Complex I in the

¹Department of Pathology and Laboratory Medicine, Emory University School of Medicine, Atlanta, GA 30322, USA; ²Department of Neurology, Renmin Hospital of Wuhan University, Wuhan, Hubei, China and ³Department of Neurology, Union Hospital, Tongji Medical College, Huazhong University of Science and Technology, Wuhan, Hubei, China

Correspondence: Xuebing Cao (caoxuebing@126.com) or Keqiang Ye (kye@emory.edu)

These authors contributed equally: Eun Hee Ahn, Seong Su Kang

Received: 14 May 2019 Accepted: 11 September 2019

Published online: 24 October 2019

muscle or brain, solely acts on enteric nervous system (ENS) and triggers α -Syn inclusions in the gut neuronal plexi that progressively spread to SN via the vagus nerve, leading to dopaminergic neuronal loss and motor disorders.²⁸

Asparagine endopeptidase (AEP) is a lysosomal cysteine protease and specifically cleaves its substrate after asparagine residues.²⁹ Recently, we reported that this enzyme is escalated in the brain in an age-dependent manner. It simultaneously cleaves both amyloid precursor protein (APP) and Tau in Alzheimer's disease (AD) brains and mediates the senile plaque and NFT (neurofibrillary tangle) pathologies.^{30,31} AEP cuts Tau at N368, and enhances the aggregation of Tau and augments its neurotoxicity. Inactivation of AEP blunts the cognitive defects and NFT pathologies in Tau P301S mice.^{30,32} Most recently, we reported that AEP is activated in PD brains, and cleaves human α -Syn at N103 and mediates its roles in PD pathogenesis. Overexpression of α -Syn N103 fragment induces LB formation and triggers motor dysfunctions.³³ In the current report, we show that α -Syn N103 fragment robustly interacts with Tau N368 fragment, which are elevated in PD patients' gut and brain. Low doses of rotenone selectively elicit p- α -Syn inclusions and constipation in young SNCA transgenic mice but not SNCA/AEP^{-/-} mice. Remarkably, rotenone-triggered α -Syn N103/Tau N368 complexes travel along the vagus nerve to the brainstem in SNCA/AEP wild-type (WT) but not SNCA/AEP-null mice, and their transportation rates are higher than full-length (FL)/FL complex PFFs, α -Syn N103 or Tau N368 PFFs individually. Interestingly, α -Syn N103/Tau N368 complex PFFs are much more potent in triggering endogenous α -Syn or Tau phosphorylation and aggregation and neuronal death than their FL/FL counterparts. Strikingly, colon-inoculated α -Syn N103/Tau N368 PFFs spread from the gut to the brain, triggering PD pathologies and behavioral deficits.

RESULTS

α -Syn N103/Tau N368 strongly interact with each other and trigger endogenous counterpart phosphorylation

To explore whether AEP cleavage regulates the interaction between Tau and α -Syn, we conducted *in vitro* binding assay employing purified recombinant proteins via Biacore. The immobilized α -Syn strongly interacted with Tau, and truncation of Tau N368 displayed stronger binding affinity toward α -Syn N103 fragment (Supplementary information, Fig. S1a, b). Moreover, we examined the interaction between α -Syn truncate and Tau fragment and their FL counterparts in intact cells. Consistent with the Biacore assay, GST pull-down revealed that the strongest binding occurred between α -Syn N103 and Tau N368 among all of the combinations (Fig. 1a, bottom). To further explore AEP's effect in catalyzing α -Syn and Tau cleavage and interaction, we tested different dosages of rotenone in dopaminergic SH-SY5Y cells for 24 h. Interestingly, rotenone induced a dose-dependent AEP enzymatic activity escalation (Supplementary information, Fig. S1c). Rotenone gradually elicited AEP cleavage and triggered α -Syn fragmentation at N103 and Tau cleavage at N368 in dopaminergic cells (Supplementary information, Fig. S1c). Immunoprecipitation showed that AEP-cleaved Tau N368 tightly interacted with α -Syn N103 upon rotenone treatment (Supplementary information, Fig. S1d). Hence, rotenone treatment induces AEP activation that subsequently cleaves both Tau and α -Syn in SH-SY5Y cells, resulting in α -Syn N103/Tau N368 complex formation.

Thioflavin T (Th-T) fibrillation kinetic assay with purified recombinant proteins showed that they formed the aggregated fibers in a time-dependent manner with α -Syn N103 + Tau N368 mixture the fastest among the combinations and they all reached the plateau on day 6 (Fig. 1b). To assess the PFF's capability in inducing fibrillization of native proteins by acting as a nidus, we tested different ratios of PFFs/native proteins. We found that PFFs from α -Syn N103/Tau N368 swiftly triggered native protein

mixture fibrillization at dilution ratio of 1:70, followed by α -Syn FL/Tau FL PFFs, whereas other combinations failed; at 1:100 ratio, none of them was able to initiate the fibrillization (Fig. 1c). However, at 1:35 and 1:10 dilution ratios, most of the PFFs induced the native monomer protein fibrillization, but α -Syn FL or Tau FL PFFs barely exhibited the seeding capability (Supplementary information, Fig. S1e). Hence, our findings suggest that α -Syn N103/Tau N368 PFFs possess the strongest seeding ability in initiating native protein filamentous fiber formation.

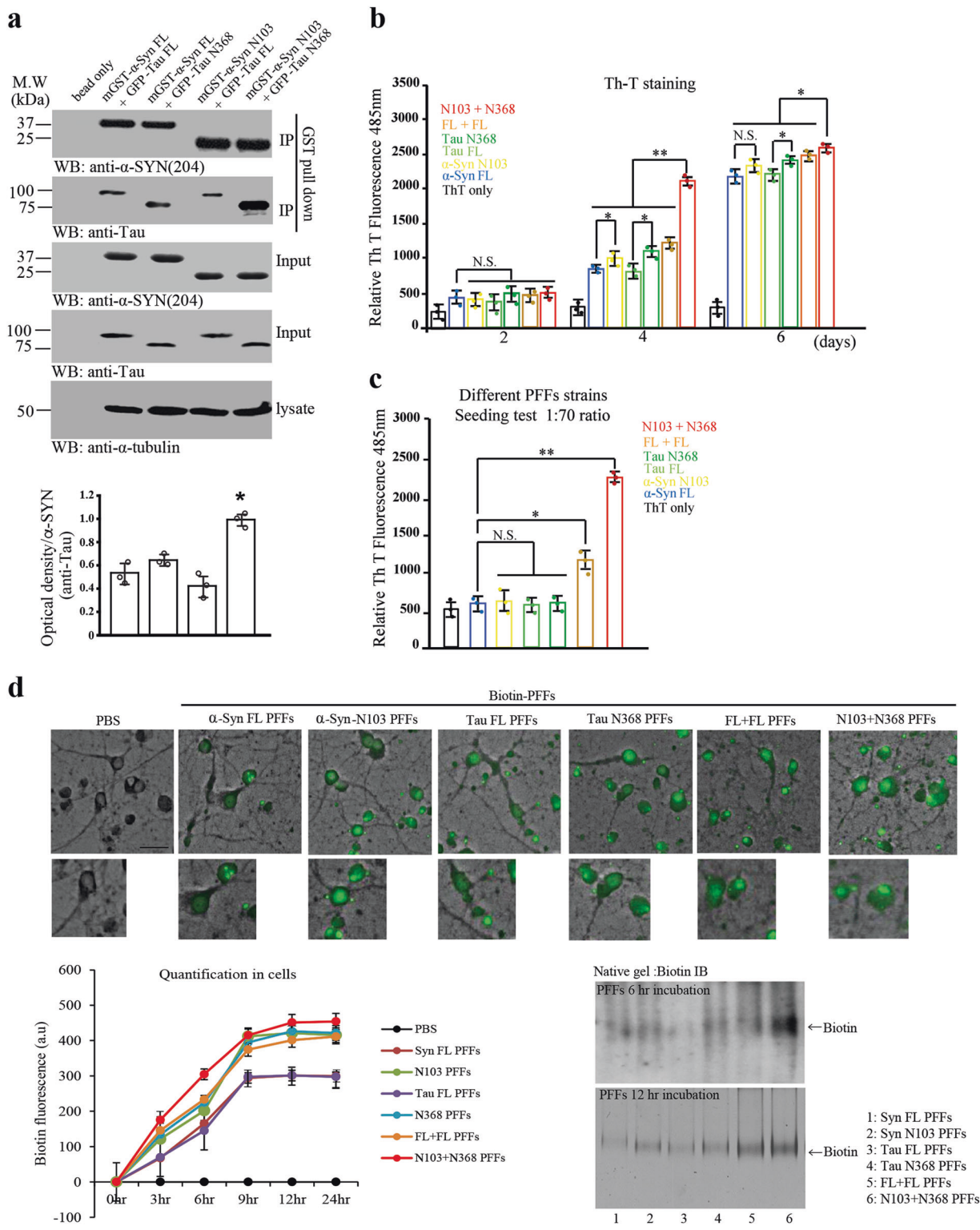
To investigate whether PFFs are cell permeable, we performed cell uptake assay of biotinylated PFF. We added 100 nM biotinylated PFFs into culture medium of primary neurons (DIV10), and monitored biotin signal 3, 6, 12, and 24 h later. Immunofluorescent (IF) staining of biotin-streptavidin revealed that intracellular signal of biotinylated PFFs was rapidly increased in α -Syn N103 + Tau N368 PFF-treated group compared to other groups (Fig. 1d). Noticeably, Tau N368 but not FL PFFs induced endogenous α -Syn S129 phosphorylation, whereas both α -Syn N103 and FL stimulated demonstrable S129 phosphorylation (Supplementary information, Fig. S2c). Hence, our findings indicate that PFFs from α -Syn N103/Tau N368 are highly cell permeable and potently induce endogenous protein phosphorylation by acting as seeds.

Biophysical and biochemical characterization of PFFs of α -Syn N103/Tau N368 complex

To assess whether the different seeding features of the PFFs reflect structural differences, we conducted a battery of biophysical and biochemical analyses. Transmission electron microscopy (TEM) showed that PFFs of α -Syn (~2.2–2.6 nm) were much thinner than those of Tau (~7.3–10.4 nm), regardless of truncation by AEP. It is worth noting that FL/FL (α -Syn/Tau) PFFs displayed ~9–10 nm thickness, whereas PFFs from α -Syn N103/Tau N368 were ~1 nm in diameter (Fig. 2a, b; Supplementary information, Fig. S2b). The fibril length analysis showed that α -Syn N103/Tau N368 PFFs (~150 nm) were significantly shorter than the other 5 PFFs (all ~500 nm in length) (Supplementary information, Fig. S2c). Together, these data suggest that PFFs (α -Syn N103/Tau N368) are much thinner and more compact than FL/FL counterpart. Proteinase K dosage assay showed that α -Syn FL fibrils were digested with the fastest rate in a dose-dependent manner, followed by Tau FL fibrils. Strikingly, PFFs (α -Syn N103/Tau N368) were the most resistant to proteinase K digestion among the 6 species (Fig. 2c). To further explore the structure difference among these different species of PFFs, we performed a limited proteolysis of equal amount of fibrils with proteinase K at 37 °C for 1 h. Notably, the fibrils of α -Syn FL, N103 and Tau FL were extensively degraded; in contrast, the main portion of the fibrils from Tau N368, FL/FL (α -Syn/Tau) and α -Syn N103/Tau N368 were intact (Fig. 2d), indicating that Tau N368 fibrils are more resistant to Protein K digestion as compared to its FL PFFs, so were PFFs of α -Syn N103/Tau N368 versus FL/FL counterpart. X-ray fiber diffraction measures the molecular structure from scattering data. The sub-structural analysis of the fibrils revealed that they all shared the similar core structures. Stalks from each sample gave rise to anisotropic X-ray diffraction patterns displaying the typical features of a cross- β substructure, with axial inter-strand reflections at ~4.4 Å for α -Syn FL, similar to α -Syn N103. However, Tau N368 fibrils exhibited more intense and characteristic anisotropic reflection than Tau FL fibrils, so did PFFs (α -Syn N103/Tau N368) as compared to FL/FL counterpart (Fig. 2e–j). Thus, α -Syn N103/Tau N368 fibrils are much denser and thinner than other fibrils.

PFFs of α -Syn N103/Tau N368 trigger aggregation of endogenous counterparts and neurotoxicity in an AEP-dependent way

To explore whether α -Syn N103 or Tau N368 PFFs induce endogenous α -Syn or Tau to form fibrils in primary neurons, we prepared primary dopaminergic neurons and cortical neurons from



WT and AEP KO neonatal pups, and pretreated neurons with 100 nM of various PFFs for 4 or 8 days, respectively. We stained tyrosine hydroxylase (TH)/MAP2 to verify dopaminergic neurons (Fig. 3a) and the treated neurons were co-stained with antibodies of MAP2/p-S129 and TH/AT8 for α -Syn and Tau pathological phosphorylation. Notably, α -Syn N103 and Tau N368 PFFs elicited evident p-S129 and AT8 signals compared to PBS control in dopaminergic neurons on day 8 (Fig. 3b, c). Nonetheless, α -Syn FL or Tau FL PFFs

only induced their own endogenous counterpart phosphorylation (Fig. 3b, c). Strikingly, α -Syn N103/Tau N368 PFFs provoked the prominent increase of both p-S129 and AT8, which were more potent than FL/FL PFFs (Fig. 3b, c). We confirmed the increase of exogenous α -Syn using Syn505 antibody, which detects human α -Syn (Fig. 3d). We quantified each antibody signal in cells (Fig. 3e). Again, these effects were time dependent with WT neurons more pronounced than AEP KO neurons. PFFs (α -Syn N103/Tau N368)

Fig. 1 α -Syn N103/Tau N368 strongly interact with each other and trigger endogenous mouse α -Syn phosphorylation in primary neurons. **a** AEP-cleaved α -Syn N103 strongly interacts with AEP-cleaved Tau N368. GST pull-down assay was performed in transfected HEK293 cells. The expression of pull-down GST- α -Syn FL and GST- α -Syn N103 and 10% input in cell lysates were shown and the expression level was quantified by densitometric analysis (bottom panel). Results are shown as means \pm SEM; $n = 3$ independent experiments; $*P < 0.05$ by two-tailed Student's *t*-test. **b** α -Syn N103 and Tau N368 complex aggregate and form fibrils the fastest among all of the strains. Thioflavin T assay showed that different aggregation rates of purified human α -Syn FL, α -Syn N103, Tau FL, Tau N368, α -Syn with Tau FL combination and AEP-cleaved fragment combination. Results are shown as means \pm SEM; $n = 3$ independent experiments; $*P < 0.05$, $**P < 0.01$ by two-tailed Student's *t*-test. **c** Seeding capacity assay. Seeding of (α -Syn N103 + Tau N368) PFFs promotes the aggregation of native proteins at 1:70 ratios. α -Syn N103 + Tau N368 aggregation (0.7 μ M) was assessed with Th-T assays in the presence of 1 (α -Syn N103 + Tau N368 fibrils, 10 nM):70 (monomers, 690 nM) ($*P < 0.05$, $**P < 0.01$). **d** Representative images of mouse middle brain neuron cells following 12-h incubation with PBS or biotinylated PFFs. The line graph is PFF uptake quantified by total cellular biotin fluorescence related time dependency (lower left panel). Uptake of 6 different PFFs (100 nM) by mouse middle brain neurons was measured by 4% native gel biotin immunoblot analysis (lower right panel). We performed three independent studies in all of experiments. Scale bar, 50 μ m

incited the strongest p-S129 and AT8 immunoreactivities time-dependently in WT neurons, which were greatly diminished in AEP-null neurons. Reintroduction of AEP into AEP-null mouse neurons rescued the effects (Supplementary information, Fig. S3a–c, e, f). Moreover, AEP was evidently upregulated and activated by the PFFs on day 8; PFFs (α -Syn N103/Tau N368) exhibited the most robust effect, whereas α -Syn FL fibrils barely activated AEP (Supplementary information, Fig. S3d). To determine whether PFF-induced phosphorylated α -Syn and Tau were in aggregated forms in primary neurons, we conducted immunoblotting using aggregated oligomer antibodies of α -Syn and Tau (5G4 and T22). Again, α -Syn N103/Tau N368 PFFs triggered more abundant higher molecular weight oligomers or aggregates with a stronger effect than FL/FL PFFs (Supplementary information, Fig. S3g). MTT analysis showed that PFF-induced cell death was tightly correlated with the same patterns as α -Syn and Tau phosphorylation in the neurons (Supplementary information, Fig. S3h). Thus, our data suggest that AEP-cleaved α -Syn or Tau fragments form the cytotoxic fibrils, which elicit α -Syn and Tau phosphorylation in a time-dependent fashion. Additionally, this effect was stronger with WT neurons than AEP-null neurons.

Chronic oral rotenone treatment initiates α -Syn N103/Tau N368 complex in the gut and brain, inducing constipation and PD pathologies in an AEP-dependent manner. Chronic treatment with a low dose of rotenone (5 mg/kg) induces α -Syn accumulation in the ENS in the gut and DMV (dorsal motor nucleus of the vagus) in the absence of detectable rotenone in the circulation system or the brain. In addition, this paradigm induces TH neuronal loss in the SN.²⁸ To test whether lower dose of neurotoxin rotenone (2.5 mg/kg) triggers AEP local activation in the ENS, we employed 3-month-old SNCA transgenic mice. After 3 months of oral administration, we performed the colon tissue section and stained with various indicated antibodies including α -Syn N103, Tau N368 and AEP. Dopaminergic neurons were labeled with TH. Strikingly, rotenone elicited evident AEP increase compared with vehicle control, accompanied with evident α -Syn N103 and Tau N368 expression and demonstrable TH cell loss (Supplementary information, Fig. S4a–d). We made the similar observations in the SN regions of SNCA transgenic mouse brain (Supplementary information, Fig. S4f–i). The quantitative analysis data were summarized in Supplementary information, Fig. S4k, l. To demonstrate whether rotenone triggered α -Syn aggregates, we stained the gut and brain sections with antibodies against α -Syn p-S129 and ubiquitin, well-characterized biomarkers for the LB inclusions. As expected, rotenone elicited demonstrable α -Syn p-S129 immunoreactivity in the gut and SN of SNCA transgenic mice (Supplementary information, Fig. S4e, j). Together, these data strongly support that rotenone triggers AEP activation and subsequent α -Syn N103 and Tau N368 fragmentation, and LB-like inclusion formation in the gut and the brain.

Next, we examined whether AEP plays any role in chronic low-dose rotenone treatment-induced motor and non-motor

symptoms. Accordingly, we employed 3-month-old SNCA/AEP WT and SNCA/AEP KO mice. After 3 months of oral administration, we monitored the motor functions by performing rotarod behavioral test. Interestingly, rotenone elicited significant motor disorders in SNCA/AEP WT but not in SNCA/AEP KO mice; however, WT mice or AEP KO mice displayed the similar motor activities without demonstrable deficits (Fig. 4a). Immunohistochemistry (IHC) of TH showed that rotenone induced substantial TH loss in SN of SNCA/AEP WT mice, and these effects were mitigated in SNCA/AEP KO mice (Fig. 4b), indicating that AEP is implicated in low-dose rotenone-triggered dopaminergic neuronal loss in the brain.

Resection of autonomic nerves abrogates chronic low-dose rotenone treatment-induced α -Syn accumulation in the ENS in the gut and progression to DMV,²⁸ indicating that LBs might transport along the vagus nerve. α -Syn is present in the human PD brain lysates, and distinct recombinant α -Syn forms are transported via the vagal nerve and reach DMV in the brainstem in a time-dependent manner after injection into the intestinal wall.²⁷ If rotenone induces AEP activation that leads to both α -Syn and Tau cleavage and complex fibrillization in the gut, one would wonder whether the complex could transport along the vagus nerve after rotenone treatment. Consequently, we performed IF and IHC staining on the vagus nerve from the intestine to the brainstem, respectively, 3 months after rotenone treatment on SNCA/AEP WT mice. IF staining with biotin-labeled α -Syn N103 antibody and Tau N368 antibody revealed that rotenone induced robust α -Syn N103 and Tau N368 signals in the vagus nerve as compared with undetectable signals in vehicle control-treated samples. Remarkably, α -Syn N103 co-localized with Tau N368, indicating that AEP-cleaved α -Syn N103 interacts with Tau N368 in the vagus nerve (Fig. 4c, d). There was no detectable α -Syn N103 or Tau N368 activity in the vagus nerves in SNCA/AEP^{−/−} mice (Fig. 4d). Hence, rotenone induces AEP-mediated formation of α -Syn N103/Tau N368 complexes that transport along the vagus nerve from the gut to the brainstem. Noticeably, rotenone triggered prominent apoptotic TH neuronal loss in an AEP-dependent manner (Fig. 4e). Immunoblotting showed that rotenone induced apparent TH loss in the colon tissues of SNCA/AEP WT but not SNCA/AEP^{−/−} mice. By contrast, serotonergic neurons (5HT2A) remained intact regardless of rotenone treatment. In agreement with these findings, α -Syn S129 was heavily phosphorylated in SNCA/AEP WT mice but weakly in SNCA/AEP^{−/−} mice. Moreover, α -Syn N103, Tau N368 and AT8 were selectively detected in SNCA/AEP WT but not SNCA/AEP^{−/−} mice (Fig. 4f). We made similar observations in the SN tissues (Fig. 4g).

Rotenone causes delayed gastric emptying and enteric neuronal dysfunction when administered chronically to rats, and it also induced slowing of GI motility.^{25,26} Accordingly, we examined the colon length, stool moisture and total GI tract transit time in SNCA/AEP WT and SNCA/AEP KO mice after 3 months of rotenone treatment. Noticeably, rotenone treatment caused evident colon length reduction, prominent decrease of stool moisture and increase of GI tract transit time in SNCA/AEP

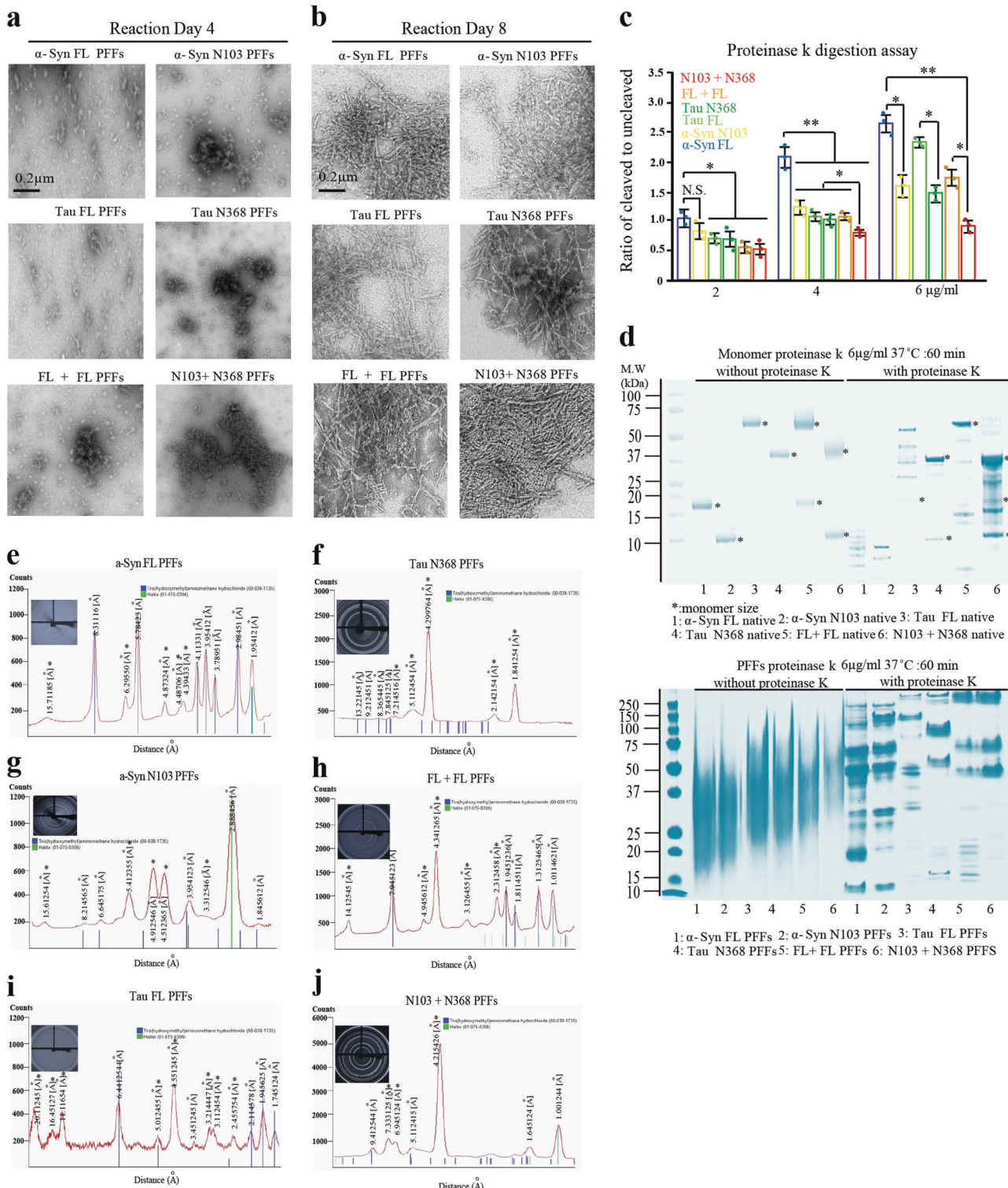


Fig. 2 Biophysical and biochemical characterization of PFFs of α-Syn N103/Tau N368 complex. **a, b** Negative stained TEM images of α-Syn FL, α-Syn N103, Tau FL, Tau N368, α-Syn FL/Tau FL, and α-Syn N103/Tau N368 on day 4 (**a**) and day 8 (**b**). Scale bar, 200 nm. **c** Quantification of proteinase K digestion rates of PFFs. The bar graph showed quantification of the relative intensity of the cleaved bands versus uncleaved band by different concentrations of proteinase K. Results are shown as means \pm SEM; $n = 3$ independent experiments; $*P < 0.05$, $**P < 0.01$ by two-tailed Student's *t*-test. **d** PFFs (α-Syn N103/Tau N368) are resistant to proteinase K digestion. Proteinase K digestion patterns of α-Syn FL, α-Syn N103, Tau FL, Tau N368, α-Syn FL/Tau FL and α-Syn N103/Tau N368 (100 μM monomer concentration), were monitored on Coomassie blue stained SDS-PAGE (18%). **e–j** X-ray diffraction pattern of partially aligned α-Syn FL (**e**), α-Syn N103 (**g**), Tau FL (**i**), Tau N368 (**f**), α-Syn FL + Tau FL (**h**) and α-Syn N103 + Tau N368 (**j**) fibrils

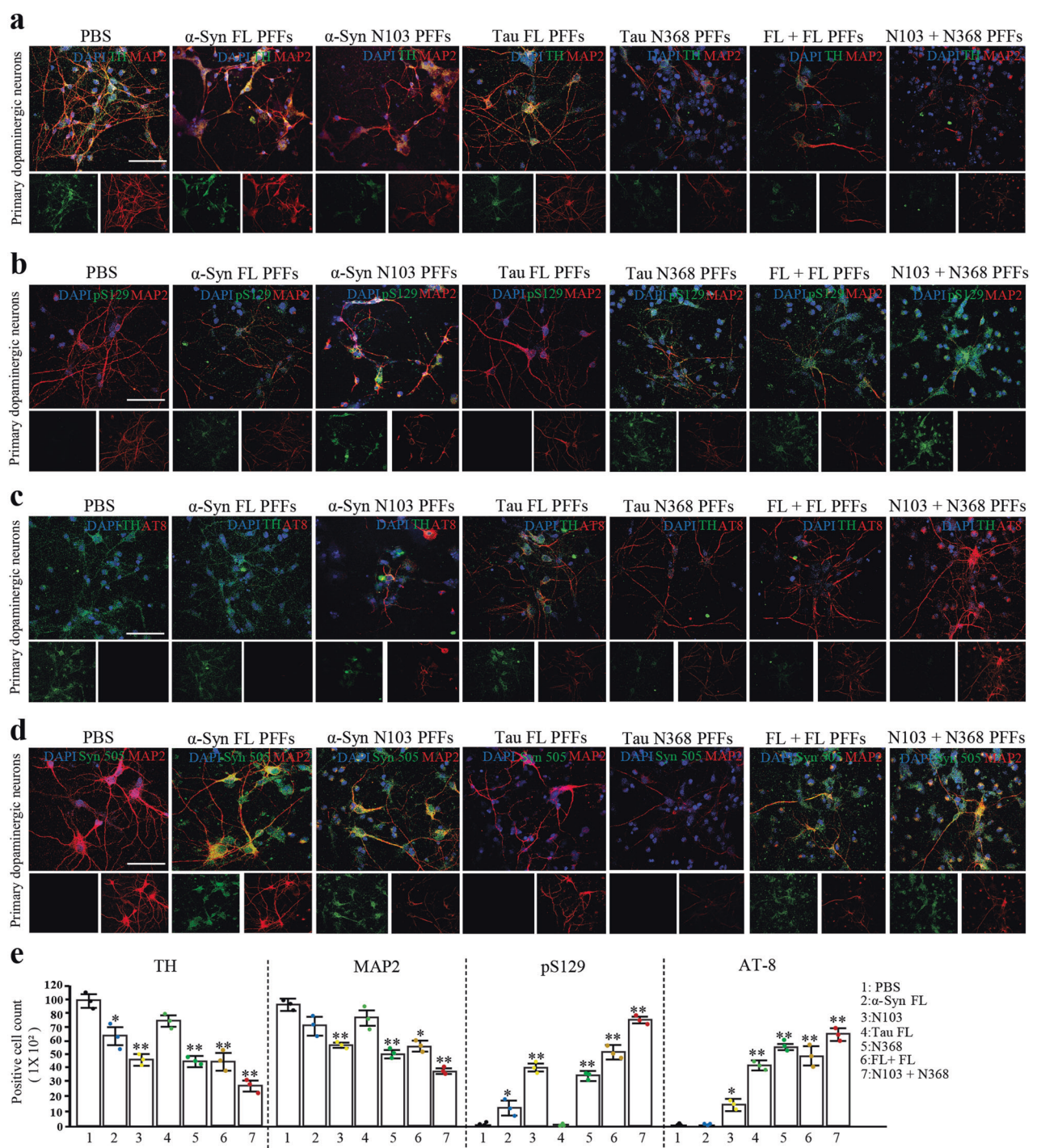
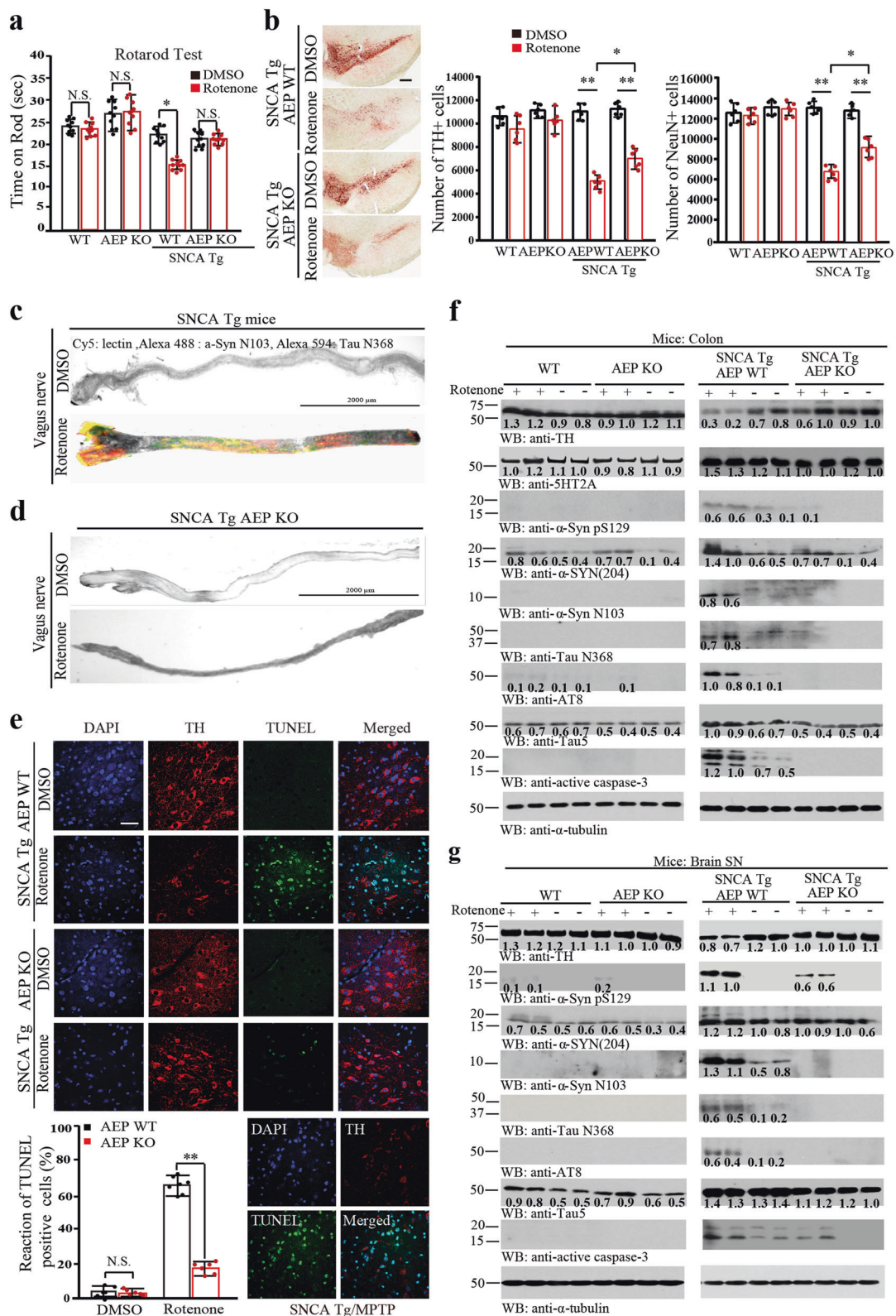


Fig. 3 PFFs of α-Syn N103/Tau N368 trigger phosphorylation of endogenous counterparts in dopaminergic neuron. **a–d** Representative images of immunofluorescent staining using TH, α-Syn p-S129, Tau phosphorylation (AT8) and mouse α-Syn (Syn505) antibodies. Primary neurons (DIV 10) were treated with 100 nM of α-Syn FL, α-Syn N103, Tau FL, Tau N368, α-Syn FL + Tau FL, α-Syn N103 + Tau N368 PFFs, and PBS for 8 days. Immunostaining showed the endogenous mouse TH, α-Syn p-S129, Tau AT8 (Ser202, Thr205) and human α-Syn expression levels with or without 6 different PFFs. Scale bar, 50 μm. **e** Quantification bar graph of TH-, MAP2-, α-Syn p-S129- and Tau AT8-positive cells. Results are shown as means ± SEM; $n = 3$ independent experiments; * $P < 0.05$, ** $P < 0.01$ by two-tailed Student's *t*-test

WT but not SNCA/AEP KO mice, whereas the constipation effects induced by rotenone were comparable between WT and AEP KO mice (Supplementary information, Fig. S5a–c). Again, IHC staining showed that rotenone elicited abundant α-Syn p-S129 immunoreactivity in the gut of SNCA/AEP WT but not SNCA/AEP KO mice (Supplementary information, Fig. S5d). HPLC analysis showed that rotenone was detectable in the gut but not in the brain tissues

(Supplementary information, Fig. S5e). These findings strongly suggest that AEP plays an important role in rotenone-induced constipation in human SNCA transgenic mice. Therefore, AEP is required for chronic low-dose rotenone treatment to trigger α-Syn and Tau pathological phosphorylation and TH loss in both the ENS and the CNS. Rotenone induces the motor dysfunction and gut mobility defects in SNCA/AEP WT but not SNCA/AEP KO mice.



AEP-cleaved α -Syn N103 and Tau N368 are augmented in PD patients' gut and brain

Braak et al. proposed that the LBs formed in the gut spread from the ENS to the CNS, the pathological manifestation that correlates well with the clinical progression of the disease. Lewy pathology first appears in enteric neurons of the gut (stage 1) long before it is present in dopaminergic neurons of the midbrain and PD

symptoms are evident (stage 3). The gap between stages 1 and 3 may take many years.³⁴ To examine whether AEP is upregulated in PD patients' brains and mediates α -Syn and Tau proteolytic cleavage, we conducted IF co-staining on SN sections of PD patients and compared with the age-matched healthy control. AEP was notably increased in TH-positive dopaminergic neurons in PD samples as compared with control, and dopaminergic

Fig. 4 Rotenone initiates α -Syn N103/Tau N368 complex formation in the gut and brain, inducing PD pathologies and motor dysfunctions in an AEP-dependent manner. **a** Motor function behavioral test. Four different mouse strains (3 months old) including WT, AEP KO, SNCA/AEP KO and SNCA/AEP WT mice were orally administered with 2.5 mg/kg of rotenone daily for 3 months ($n = 10$ mice per group; * $P < 0.05$, two-way ANOVA). **b** Chronic low-dose rotenone treatment triggers dopaminergic neuronal loss in the brain. Left panel, TH immunostaining of the brain SN region tissues of SNCA/AEP WT and SNCA/AEP $^{−/−}$ mice. Scale bar, 200 μ m. Right panels, bar graph of stereologically counted TH and NeuN-positive cells. Results are shown as means \pm SEM; $n = 6$ independent experiments; * $P < 0.05$, ** $P < 0.01$ by two-way ANOVA. **c, d** Rotenone induces α -Syn and Tau cleavage and the complex travels along the vagus nerve. α -Syn N103 and Tau N368 were co-immunostained in the vagus nerve of SNCA transgenic mice but not SNCA/AEP $^{−/−}$ mice (Cy5-gray, lectin; Alexa 488-green, α -Syn N103; Alexa 594-red, Tau N368). Scale bar, 2 mm. **e** TUNEL staining of TH-positive cells in SN of SNCA/AEP mice. Rotenone induced more TUNEL-positive TH cell death in SNCA/AEP WT mice than SNCA/AEP $^{−/−}$ mice. The bottom right panel is positive control for TUNEL staining of MPTP-treated SNCA transgenic mice. Scale bar, 50 μ m. Bar graph in bottom left panel shows the quantification of TUNEL-positive cells. $n = 6$ each group; ** $P < 0.01$, Student's *t*-test. **f** Rotenone induces TH apoptotic loss and AEP activation in the gut of SNCA but not SNCA/AEP $^{−/−}$ mice. Representative immunoblotting images showed the expression of TH, 5HT2A, α -Syn p-S129, truncated α -Syn, Tau and p-Tau AT8 and active caspase-3 in the colon. α -tubulin is loading control. **g** Rotenone induces TH apoptotic loss and AEP activation in the SN of SNCA but not SNCA/AEP $^{−/−}$ mice. Immunoblotting showed the expression of TH, α -Syn p-S129, truncated α -Syn and Tau, Tau AT8 and active caspase-3 in the SN. α -tubulin is loading control. All of experiments were performed three times independently

neurons were prominently reduced (Fig. 5a, top left side). Consequently, Tau N368 and α -Syn N103 were highly elevated and co-localized in PD patients, whereas these IF signals were barely detectable in healthy controls (Fig. 5a, right side). To investigate whether the similar phenomena occurred in the GI tract, we prepared PD patients' and healthy controls' sections from colon tissue biopsy. Compared to the control, AEP was greatly augmented in PD patients' gut, and some of AEP co-localized with TH-positive dopaminergic submucosal neurons (Fig. 5b, bottom right side). IF co-staining demonstrated that α -Syn N103 and Tau N368 co-localized in the Patients' gut (Fig. 5b, middle and bottom left sides). Therefore, our data support that AEP is activated in both the gut and the brain of PD patients, cleaving Tau and α -Syn in dopaminergic neurons.

Colon-injected PFFs of α -Syn N103/Tau N368 complex progress to the brainstem along the vagus nerve
Rotenone induces constipation in SNCA transgenic mice in an AEP-dependent manner (Supplementary information, Fig. S5a–c). Moreover, we observed the LB-like inclusions that consist of α -Syn N103 and Tau N368 truncates in SNCA but not SNCA/AEP $^{−/−}$ mouse's gut, transporting from the gut to the brain along the vagus nerve (Fig. 4). We wondered whether colon-injected PFFs of α -Syn N103/Tau N368 complex translocate from the colon to the brainstem, which may subsequently spread to the SN or other synaptically interconnected brain regions, resulting in dopaminergic neuronal loss and a variety of behavioral abnormalities. To test this possibility, we employed 3-month-old SNCA transgenic mice and injected different species of biotinylated PFFs via colonoscopy, and monitored PFF transportation along the vagus nerve at subsequent time points. Noticeably, different PFFs exhibited differential traveling rates along the nerve with α -Syn N103/Tau N368 > α -Syn N103 > Tau N368. PFFs (α -Syn N103/Tau N368) reached the brainstem first from the colon within 9 days, followed by α -Syn N103 (10 days), FL/FL and Tau N368 (12 days), respectively (Supplementary information, Fig. S6a–f). To assess whether AEP plays any role in mediating PFF transportation along the vagus nerve, we conducted the same experiments in age-matched SNCA/AEP $^{−/−}$ and WT mice. We found that knockout of AEP slowed down the travel speed of PFF (α -Syn N103/Tau N368), which reached the brainstem after 12 days, and its speed was similar to that of WT mice (Supplementary information, Fig. S6g, h), indicating that AEP somehow participates in PFF transportation. Moreover, spinal cord staining failed to detect the colon-injected PFFs, indicating that the PFFs are primarily transported via the vagus nerve (Supplementary information, Fig. S6c–h). To explore whether colon-inoculated PFFs induce any α -Syn or Tau pathologies in the brainstem via the vagus nerve, we resected the truncus vagalis anterior on one side (hemivagotomy). Two days after inoculation of biotinylated PFFs (α -Syn N103/Tau N368) into

the gut wall, we performed the surgery. In 1 week, we conducted IHC to examine Tau and α -Syn phosphorylation in NTS (nucleus tractus solitarius) or DMV region using anti-AT8 or anti-p-S129 antibody, respectively. Interestingly, we found that AT8 signals were strongly elevated in NTS region in the intact side, whereas no signal was detected in the side where vagus nerve was resected. IF co-staining with anti-biotin and anti- α -Syn N103 antibodies showed that α -Syn N103 and Tau N368 co-localized in the sensory nerve cell body (Supplementary information, Fig. S7a). α -Syn p-S129 immunoreactivities were highly augmented in DMV region of the uncut side, but not detectable in the cut side. Again, IF co-staining revealed that α -Syn N103 and Tau N368 co-localized in the neurons of DMV (Supplementary information, Fig. S7b). Thus, colon-inoculated PFFs can spread along the vagus nerve to the brain, and hemivagotomy eliminates PFF-induced α -Syn or Tau pathologies on the same side of the brainstem. IF co-staining with biotin and α -Syn p-S129 antibodies showed that intrastriatally injected PFFs (α -Syn N103/Tau N368) induced potent p-S129 immunoreactivities in dopaminergic neurons in the SN region of WT mice (Supplementary information, Fig. S7c). We made the similar observations with colon-inoculated PFFs (α -Syn N103/Tau N368), which provoked robust p-S129 signals in neurons in DMV of SNCA transgenic mice (Supplementary information, Fig. S7d). The induced p-S129 signals surrounded exogenous biotinylated PFFs, indicating that the injected PFFs act as seeds and trigger endogenous α -Syn phosphorylation in the neurons in both SN and DMV. These findings were further validated by immunoblotting with samples from proteinase K digestion and insoluble fractionation (Supplementary information, Fig. S7e, g). Vagotomy was verified by H&E staining and cell counting of DMV. Cells at cut-side DMV were decreased by ~50% in one month due to inactivation of the vagus nerve (Supplementary information, Fig. S7f).

Colonic injection of PFFs of α -Syn N103/Tau N368 complex elicits PD pathologies and behavioral disorders

To investigate whether colon-inoculated PFFs that translocate to the brainstem spread to different brain regions and initiate α -Syn and Tau pathologies, we performed IHC staining with anti- α -Syn p-S129 and anti-AT8 antibodies on different brain sections of SNCA transgenic mice. Three months after injection of various PFFs, we found that p-S129 immunoreactivities were evident in DMV, SN and striatum for PFFs (α -Syn N103/Tau N368), and the activities were weaker for FL/FL PFF samples. However, only negligible p-S129 immunoreactivities were detected in α -Syn N103 PFF group or PBS-treated control group. By contrast, no p-S129 immunoreactivities were detected for Tau N368 PFFs in these regions (Fig. 6a, right panels). The schematics for p-S129 signals was summarized (Fig. 6a, left panels). Since NTS nerves project into the Locus Coeruleus (LC) and hippocampus (HC) regions, we monitored AT8 signals in these regions accordingly.

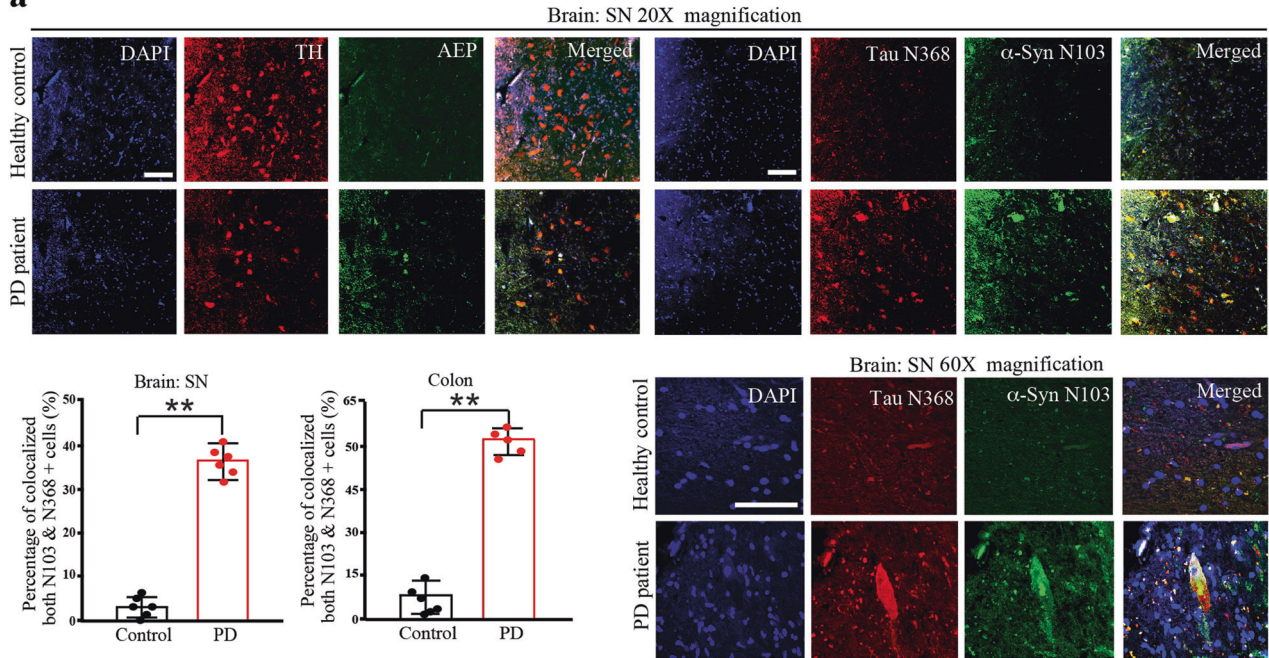
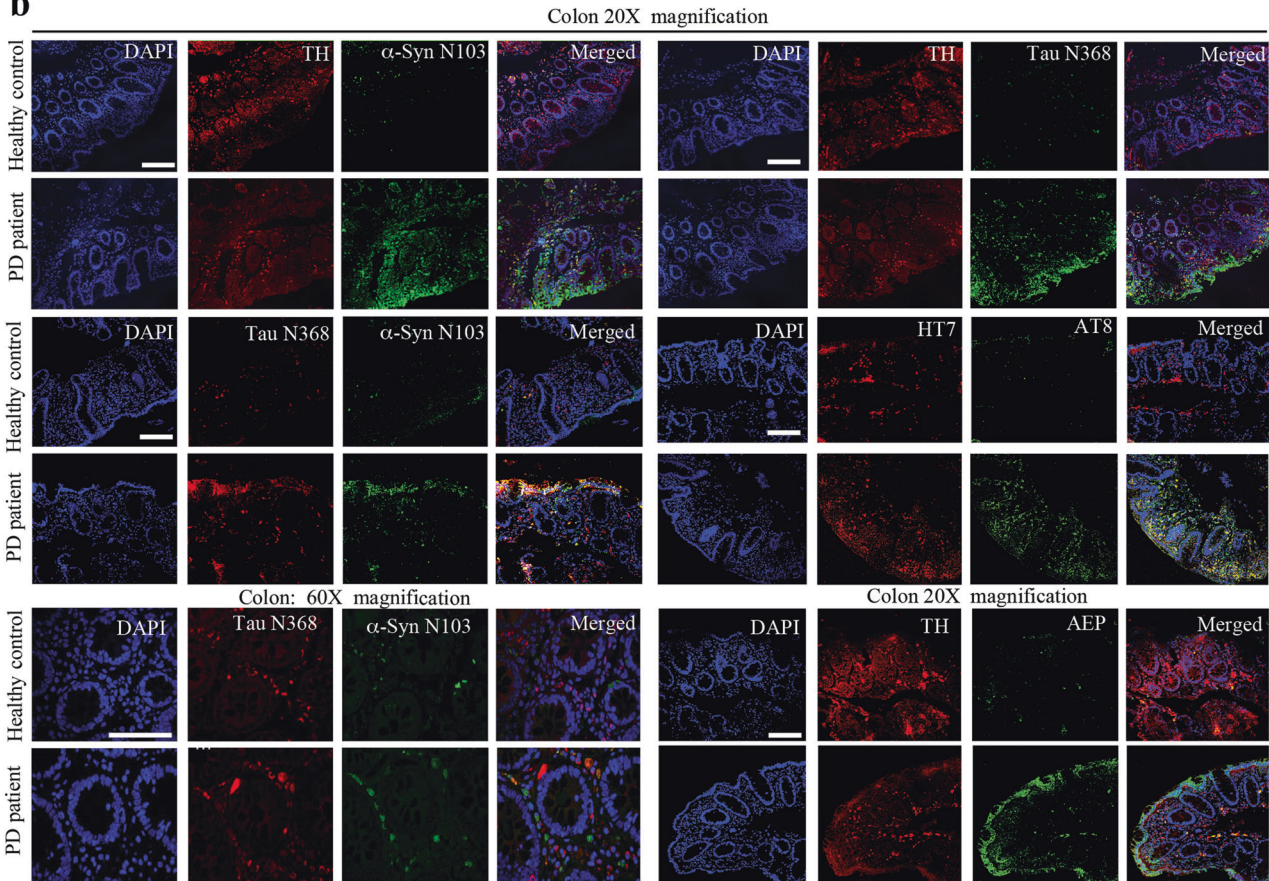
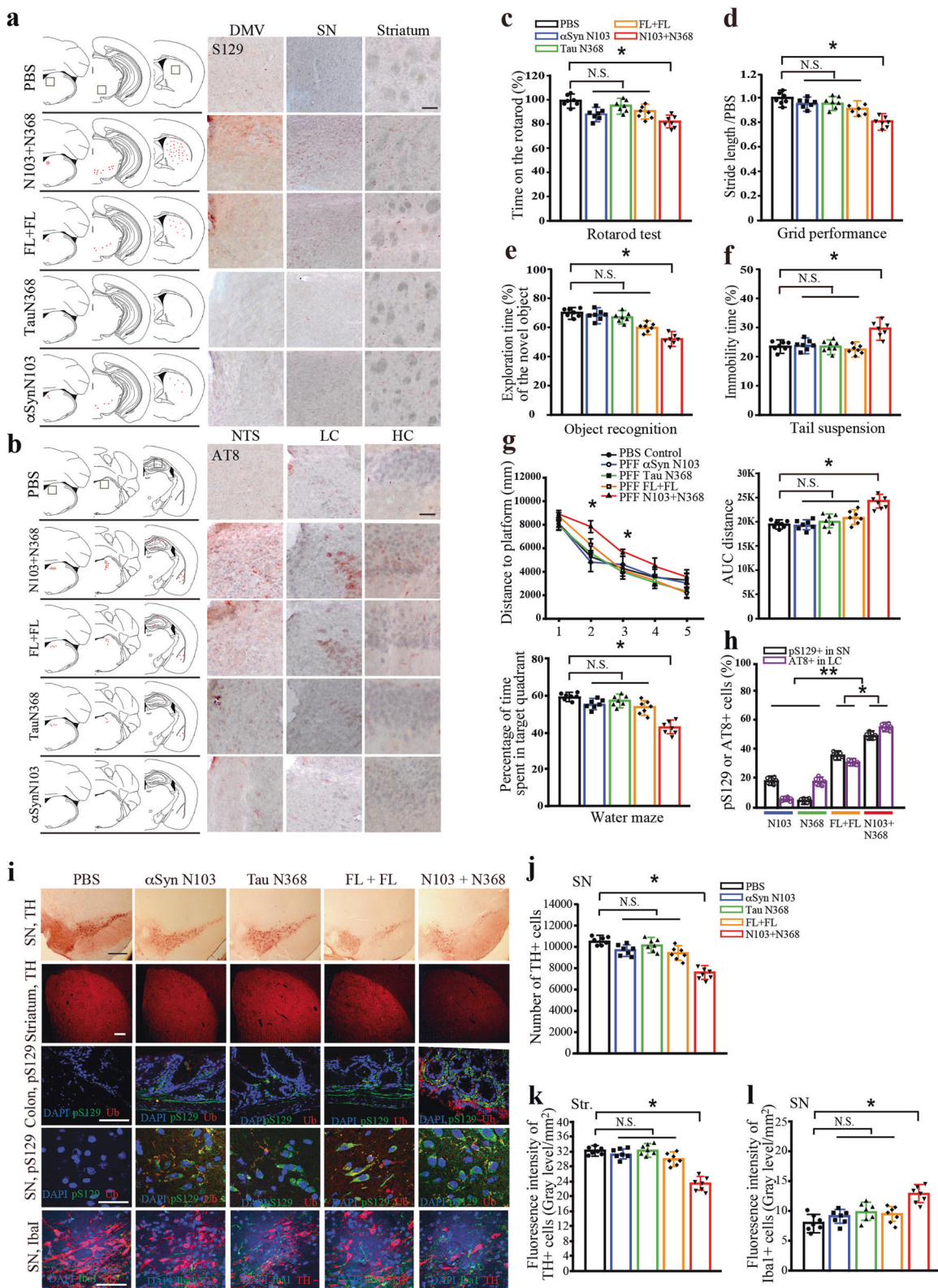
a**b**

Fig. 5 AEP-cleaved α -Syn N103 and Tau N368 are augmented in PD patients' gut and brain. **a** Immunostaining showed AEP (green) and TH (red) expression levels in the brains (SN) of the age-matched healthy control and PD patient. Immunofluorescent staining showed α -Syn N103 (green) and Tau N368 (red) co-localization in the PD patient's SN. Scale bar, 200 μ m. Quantification showed the increase of α -Syn N103 and Tau N368 co-localized cells in PD patient's SN in the lower bar graph. $n = 6$ sections each from 4 patients and 4 healthy controls; ** $P < 0.01$. **b** AEP and TH immunofluorescent staining of colons of age-matched healthy control and PD patient. Immunofluorescent staining showed that α -Syn N103 (green) and Tau N368 (green) were co-localized with TH (red) in the PD patient's colon. Scale bar, 200 μ m. Quantification of dopaminergic neurons with α -Syn N103 and Tau N368 co-localization in PD patient's colon in the lower bar graph of **a**. $n = 6$ sections each from 4 patients and 4 healthy controls; ** $P < 0.01$.



Strikingly, PFFs (α -Syn N103/Tau N368) elicited prominent Tau phosphorylation in these regions, and the activities were weaker for FL/FL PFFs, which predominantly induced AT8 signal in LC. Tau N368 PFFs exhibited the similar pattern with substantially diminished activity. However, α -Syn N103 PFFs or PBS control failed to induce any AT8 signal in any of these regions (Fig. 6b). The staining results of p-S129 and AT8 were quantified (Fig. 6h).

The total α -Syn and Tau and their aggregates were validated from both soluble and insoluble fractions (Supplementary information, Fig. S7g).

To explore whether colon-inoculated PFFs cause any behavioral disorders, we performed motor function, cognitive function and depression-like activity assays 3 months after the gut injection. Rotarod and grid performance behavioral test showed that PFFs

Fig. 6 Colonic injection of PFFs of α -Syn N103/Tau N368 complex elicits PD pathologies and behavioral disorders. **a** α -Syn pathology spread in the interconnected brain regions of dopaminergic neurons of SNCA mice 3 months after the colonic injection of the sonicated PFFs. Brain sections of DMV-SN-Striatum were immunostained by anti- α -Syn p-S129 antibody. Scale bar, 200 μ m. In the left brain atlas, the marked red dots in every spot containing positive cells show the spreading, which is the frame of 50 \times 50 μ m in size under microscope. **b** Tau pathology was detected in the synaptically connected brain regions of noradrenergic neuron of SNCA transgenic mice 3 months after the colonic injection of PFFs. Brain sections of NTS-LC-HC were examined by anti-AT8 immunohistochemistry. Scale bar, 200 μ m. **c-g** The complex PFFs (α -Syn N103/Tau N368) induced motor defects and memory deficits 3 months after the colonic injection. Motor behavioral assays, rotarod (**c**), grid performance (**d**), object recognition (**e**), tail suspension (**f**), and water maze tests (**g**) were conducted. Data are shown as means \pm SEM. $n = 7$ each group; * $P < 0.05$. **h** p-S129-positive cells in SN of **a** and AT8-positive cells in LC of **b** were quantified by counting. Data are shown as means \pm SEM. $n = 7$ each group; * $P < 0.05$, ** $P < 0.01$. **i** TH cell loss in SN and striatum of the above animals was analyzed by immunohistochemistry and immunofluorescence staining. Scale bar, 200 μ m. α -Syn aggregates in SN were confirmed by anti- α -Syn p-S129 and anti-ubiquitin immunofluorescent staining. Scale bar, 50 μ m. Neuroinflammation was verified by anti-Iba1 immunofluorescent staining. Scale bar, 50 μ m. **j, k** Quantification of TH-positive cells in the SN by stereological analysis (**j**) and fluorescence intensities of TH-positive cells in striatum (**k**). Data are shown as means \pm SEM. $n = 7$ each group; * $P < 0.05$. **l** Fluorescence intensity of Iba1-positive cells in the SN was quantified by ImageJ. Data are shown as means \pm SEM. $n = 7$ each group; * $P < 0.05$

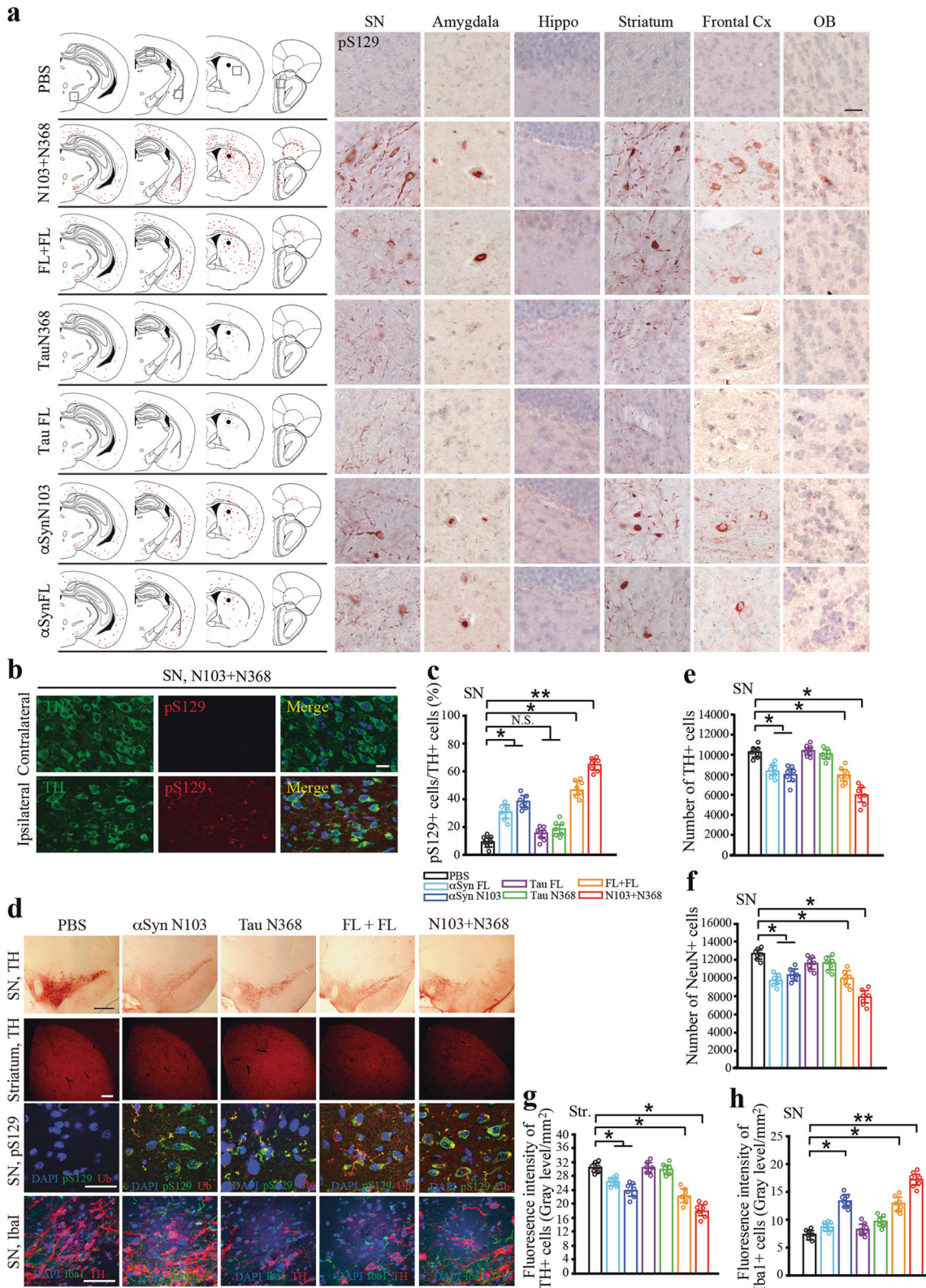
(α -Syn N103/Tau N368) elicited significant motor deficits, whereas the other 3 groups (α -Syn N103 PFFs, Tau N368 PFFs, FL/FL PFFs) remained comparable to vehicle group (Fig. 6c, d). Moreover, the tail suspension assay demonstrated that mice inoculated with PFFs (α -Syn N103/Tau N368) exhibited significantly longer immobility duration (Fig. 6f), indicative of depression-like behaviors. In addition, novel object recognition test showed that α -Syn N103/Tau N368 PFF-injected mice spent significantly less exploration time with much lower discrimination index as compared to vehicle control or the other 3 PFF groups (Fig. 6e), suggesting cognitive dysfunction. Further, Morris water maze (MWM) assay revealed that the cognitive functions were substantially impaired in SNCA mice with colonic inoculation of PFFs (α -Syn N103/Tau N368). They swam a much longer distance to locate the hidden platform submerged under water and spent significantly less time in the target quadrant; in contrast, the other 3 groups were indistinguishable from the vehicle control group (Fig. 6g). IHC staining of TH and quantification of dopaminergic neurons in SN by stereological analysis, and fluorescent intensities in striatum sections from SNCA mice inoculated with different species of PFFs indicated that dopaminergic neurons were pronouncedly reduced in the samples from PFF (α -Syn N103/Tau N368) group, whereas the other 3 PFF groups exhibited similar numbers of dopaminergic neurons to vehicle control group (Fig. 6i-k). IF co-staining with antibodies against both α -Syn p-S129 and ubiquitin showed that there were extensive LB-like inclusions in both the colon and SN of SNCA mice 3 months after colonic inoculation of PFFs (α -Syn N103/Tau N368) compared to vehicle control. Nonetheless, the LB-like inclusions were sparse in the colons from PFFs of FL/FL, Tau N368 and α -Syn N103 (Fig. 6i). Remarkably, the inclusions were also demonstrable in SN from PFFs of FL/FL and α -Syn N103. In contrast, p-S129 immunoreactivities were clearly weaker in Tau N368 PFF-injected samples (Fig. 6i). Noticeably, neuroinflammatory signal shown by Iba1 immunoreactivity was highly increased in α -Syn N103/Tau N368 group (Fig. 6i, bottom panel, and l). Therefore, our data strongly support that colon-inoculated PFFs (α -Syn N103/Tau N368) transport from the gut to the brainstem, from where they spread to the synaptically interconnected brain regions, inducing the pathological alterations of endogenous α -Syn and Tau. Subsequently, they initiate PDD (Parkinson's disease dementia)-like behaviors.

AEP enzymatic assay showed that colon-injected PFFs (α -Syn N103/Tau N368) strongly provoked AEP activation in both colon and SN regions of SNCA mice as compared to vehicle PBS (Supplementary information, Fig. S8a). As expected, activated AEP leaked out of LAMP1-positive lysosomes in both tissues, where active AEP presumably got access to its substrates in the cytoplasm (Supplementary information, Fig. S8b). Remarkably, AEP was highly escalated by PFFs (α -Syn N103/Tau N368) in both SN and colon in SNCA/AEP^{+/+} mice, co-localizing with p-S129 and AT8 as compared to PBS-injected samples (Supplementary

information, Fig. S8c, e). However, PFFs (α -Syn N103/Tau N368) lost the stimulatory effect in augmenting AEP in SNCA/AEP-null mice. Consequently, both p-S129 and AT8 signals were significantly weaker than those in SNCA/AEP^{+/+} mice (Supplementary information, Fig. S8d, f). Therefore, colon-inoculated PFFs (α -Syn N103/Tau N368) transport along the vagus nerve to the brainstem, and they induce much stronger AEP activation and endogenous α -Syn and Tau pathological alteration in both SN and colon of SNCA/AEP^{+/+} mice than SNCA/AEP-null mice.

Intrastratal inoculation of α -Syn N103/Tau N368 PFFs initiates α -synucleinopathy in mice

The dorsal striatum is interconnected with multiple CNS nuclei, including midbrain dopaminergic neurons.^{35,36} To explore whether the different species of PFFs spread to different brain regions and trigger TH-positive neuronal loss in SN after inoculation into striatum, we employed WT mice (2–3 months old) and performed IHC with anti- α -Syn p-S129 antibody on the coronal brain sections 3 months after single inoculation. Remarkably, we found that α -Syn N103/Tau N368 PFFs elicited pronounced α -Syn p-S129 pathology that was spreaded to most of the anatomically interconnected regions including SN, amygdala, frontal cortex (Cx) and Olfactory bulb (OB) but not hippocampus (Hippo). These effects were weaker with FL/FL counterpart. We made the similar observations with both α -Syn N103 and α -Syn FL PFFs (Fig. 7a). Noticeably, these PFFs failed to induce S129 phosphorylation in OB (Fig. 7a, right panels). By contrast, Tau N368 PFFs weakly triggered S129 phosphorylation in both striatum and SN and their activities were stronger than Tau FL PFFs. Both of the species failed to induce any demonstrable p-S129 signal in any other regions. The spreading schematics by these PFFs were summarized with red spots (Fig. 7a, left panels). Because the nigrostriatal pathway is exclusively unilateral, LB/LN or NFT pathology in the SNpc is confined to the injected hemisphere at all time points examined. As expected, α -Syn N103/Tau N368 PFF-elicited S129 phosphorylation was prominently elevated in the ipsilateral but not contralateral SN region (Fig. 7b). Quantitative analysis of p-S129-positive dopaminergic neurons in SN showed that α -Syn N103/Tau N368 PFFs displayed the strongest effect, followed by FL/FL PFFs that exhibited more robust effect than both α -Syn N103 and FL PFFs. The activity patterns tightly coupled with IHC staining data (Fig. 7c). IHC and IF staining against TH in both SN and striatum revealed that dopaminergic neurons were significantly lost after striatal inoculation of α -Syn N103/Tau N368 PFFs. As expected, extensive p-S129 immunoreactivity was detected in the SN injected with PFFs (α -Syn N103/Tau N368) and other PFFs (Fig. 7d). The inflammatory microglial Iba1 immunoreactivities were robustly escalated in samples inoculated with Tau-containing PFFs (Fig. 7d, bottom panel, and h). The TH loss stimulatory activities were closely correlated with p-S129 signals in both regions (Fig. 7d-g).



In addition to examination of α -Syn pathology spreading to different brain regions after intrastriatal inoculation of different species of PFFs, we also conducted AT8 IHC staining. Notably, p-Tau activity was only detected in the injected striatum with the signal intensity order: α -Syn N103/Tau N368 > FL/FL > Tau N368 > Tau FL (Supplementary information, Fig. S9a). Interestingly, α -Syn

PFFs did not elicit any detectable AT8 signals, consistent with their negative effects on endogenous Tau in primary neurons (Fig. 3b, c; Supplementary information, Fig. S3a, b). To explore whether striatal inoculation of the indicated PFFs elicit any behavioral consequences, we performed different behavioral tests including motor function, cognitive function and depression assays

Fig. 7 Intrastratal inoculation of α -Syn N103/Tau N368 PFFs initiates α -synucleinopathy in mice. **a** The PFFs injected into the striatum spread to other interconnected brain regions. Various strains of PFFs were injected into the striatum of WT mice. After 3 months, the mice were sacrificed and the brain sections were immunostained with anti- α -Syn p-S129 antibody. The spreading was confirmed by anti- α -Syn p-S129 immunohistochemistry and shown by the schematics with red dots. PFFs except Tau and Tau N368 were spreaded to the synaptically connected brain regions including striatum, SN, amygdala, and cortex. However, the expression of α -Syn p-S129 was not shown in hippocampus of any group. The α -Syn pathology was detected in the SN 3 months after α -Syn N103/Tau N368 complex PFF injection into the striatum. Scale bar, 50 μ m. **b** α -Syn pathology was detected in the SN 3 months after α -Syn N103/Tau N368 complex PFF injection into the striatum. α -Syn p-S129 expression in the SN was examined by immunofluorescent staining. Scale bar, 20 μ m. **c** α -Syn p-S129-positive cells in SN of each group were quantified by counting. Data are shown as means \pm SEM. $n = 7$ each group; * $P < 0.05$, ** $P < 0.01$. **d** TH cell loss in SN and striatum of the above animals was analyzed by immunohistochemistry and immunofluorescence staining (Scale bar, 200 μ m), and α -Syn aggregates of SN were confirmed by anti- α -Syn p-S129 and anti-ubiquitin immunofluorescent staining (Scale bar, 50 μ m). Neuroinflammation was verified by anti-Iba1 immunofluorescent staining (Scale bar, 50 μ m). **e**, **f** Quantification of TH- and NeuN-positive cells in SN by stereological analysis. **g** Fluorescence intensity of TH-positive cells in the striatum was quantified by ImageJ. Data are shown as means \pm SEM. $n = 7$ each group; * $P < 0.05$. **h** Fluorescence intensity of Iba1-positive cells in the SN was quantified by ImageJ. Data are shown as means \pm SEM. $n = 7$ each group; * $P < 0.05$, ** $P < 0.01$

3 months after intrastratal inoculation of PFFs. Rotarod behavioral test showed that only α -Syn N103/Tau N368 PFFs displayed significant motor deficits among the tested groups (Supplementary information, Fig. S9b). Since the hippocampus was not affected by the striatally inoculated PFFs, neither MWM nor novel object recognition assay exhibited any cognitive deficits (Supplementary information, Fig. S9c, d). Moreover, in alignment with the relatively sparing mesolimbic projections, no significant differences were found in any of the PFF-treated mice in tail suspension test, a measure of depression-like behavior (Supplementary information, Fig. S9e). Hence, PFFs from complex of AEP-cleaved α -Syn N103/Tau N368 possess the strongest prion-like activity among the different species of PFFs, initiating dopaminergic neuronal loss and motor deficits.

DISCUSSION

In the present study, we show that AEP cleavage of both Tau and α -Syn enhances their interaction. Notably, α -Syn N103/Tau N368 complex PFFs are much more neurotoxic than FL/FL counterparts or the individual fragments' fibrils. Interestingly, chronic low-dose rotenone treatment elicits constipation and motor deficits in SNCA/AEP^{+/+} but not SNCA/AEP^{-/-} mice, robust α -Syn and Tau cleavage, and LB-like inclusion formation in the gut, which spread along the vagus nerve to the brain, suggesting that AEP is critical for rotenone-induced PD pathogenesis. Strikingly, we found that preformed α -Syn N103/Tau N368 complex fibrils injected into the gut wall via colonoscopy travel along the vagus nerve to the brainstem, and further transmit α -Syn and Tau pathology in the synaptically interconnected regions within the brain, leading to motor dysfunctions, cognitive defects and depression-like behaviors, which are the symptoms seen in PDD patients. These findings support that rotenone-activated AEP mediates p- α -Syn aggregate inclusions in the colon, regulating its transportation from the gut to the brain. Remarkably, PFFs (α -Syn N103/Tau N368) act as seeds to induce endogenous Tau or α -Syn phosphorylation and aggregation within neurons and lead to cell-to-cell transmission of pathologies in anatomically interconnected regions after intrastratal or colonic inoculation. We detect that AEP is highly escalated in PD patients' gut and brain, accompanied by augmentation of both α -Syn N103 and Tau N368 truncates. These observations demonstrate that the hybrid aggregation is clinically relevant to PD pathogenesis.

Previous study shows that the microtubule-binding domain in Tau interacts with C-terminus (a.a. 87–140) of α -Syn.¹² Conceivably, truncating the C-terminus of Tau by AEP may reveal its microtubule-binding domain to the exposed motif (a.a. 87–103) on α -Syn N103 fragment, resulting in tighter interaction between the two AEP-cleaved fragments and stronger fibrilization (Fig. 1). X-ray diffraction shows that Tau FL and N368 PFFs are much thicker than those of α -Syn, however, α -Syn N103/Tau N368

complex PFFs are much thinner than their FL/FL or individual PFFs (Supplementary information, Fig. S2b). Conceivably, α -Syn N103 interacts with Tau N368 and changes the complex folding conformations, resulting in a much denser stacking morphology, which might shed light into their potent spreading and progressive activities. Moreover, proteinase K degradation pattern shows that α -Syn N103/Tau N368 crossbreed fibrils are different from the separate α -Syn N103 or Tau N368 fibrils. Therefore, both proteinase K digestion and X-ray diffraction reveal that α -Syn N103 and Tau N368 form the hybrid fibrils in the same fibrils by interacting with each other, instead of two separate fibrils mixed in the same sample (Fig. 2c, e–j). Surprisingly, we found that the seeding capability of α -Syn N103/Tau N368 complex PFFs is much stronger than that of FL/FL or their individual PFFs (1:70; 1:35; 1:10) (Fig. 1c and Supplementary information, Fig. S1e).

Neurotoxin-induced models provide a suitable approach to study various symptoms of PD that derive from the loss of nigrostriatal dopaminergic neurons, a cardinal feature of PD. They also include some non-motor symptoms (NMSs), primarily cognitive dysfunctions.³⁷ It has been reported that chronic rotenone administration alters the cognition in rats.³⁸ In addition, the rat may also display depressive behavior in a forced swim and sucrose preference task.³⁹ GI dysfunction is the most common NMS of PD. It has been reported that rotenone causes delayed gastric emptying and enteric neuronal dysfunction when administered chronically to rats.²⁶ Rotenone also induces an acute reduction in α -Syn-immunoreactivity, followed by a robust increase 6 months later in aggregate pathology and cytoplasmic inclusions, similar to enteric LBs in idiopathic PD. Rotenone-treated rats also display a moderate but permanent loss of small intestine myenteric neurons and modest slowing of GI motility.²⁵ Accordingly, we examined the colon length, stool water content and total GI tract transit time. Noticeably, local rotenone treatment caused evident colon length reduction, accompanied with prominent decrease of stool moisture and increase of GI tract transit time in SNCA/AEP WT but not SNCA/AEP KO mice, whereas no demonstrable GI dysfunctions were induced by chronic low-dose rotenone administration in either WT or AEP KO mice (Supplementary information, Fig. S5a–c). The shortened colon indicates the impairment of the proper functioning of the intestine including absorption of nutrients and water. Though rotenone triggers activation of numerous proteases, it barely induced α -Syn S129 phosphorylation and dopaminergic neuronal loss in SNCA/AEP^{-/-} mice (Fig. 4), suggesting that AEP is crucial for mediating rotenone-incurred PD pathologies. Thus, these findings strongly suggest that AEP plays a critical role in rotenone-induced NMSs in human SNCA transgenic mice.

α -Syn-related neurodegeneration in the ENS is a frequent and likely premotor manifestation of PD, and is associated with chronic constipation and pathophysiological changes in the intestinal wall. Consequently, aggregated α -Syn present in human PD brain

lysates, or as distinct recombinant α-Syn forms, are transported via the vagal nerve and reach DMV in the brainstem in a time-dependent manner after injection into the intestinal wall.²⁷ Different α-Syn forms can propagate from the gut to the brain, and microtubule-associated transport is involved in the retrograde translocation of aggregated α-Syn from enteric neurons. Thus, the vagus nerve could be a conduit of α-Syn-related neuropathology from the ENS to the CNS. The finding of LBs in the intestinal enteric nerves led to the hypothesis that the intestine might be an early site of PD pathologies that travel to the brain later.^{40,41} Previous studies indicate that the local effect of an environmental toxin-like rotenone on the ENS is sufficient to reproduce Braak's staging in mice. Rotenone is not detectable in either circulation system or the brain after oral administration (2.5 mg/kg) (Supplementary information, Fig. S5e), suggesting that intragastric rotenone exerts the pathological effects locally.²⁸ Nevertheless, we cannot exclude the possibility that its faint metabolites might penetrate into the brain and trigger α-Syn pathologies. To explore whether AEP cleavage of α-Syn or Tau in the gut plays any role in rotenone-elicited PD pathologies, we treated WT, AEP KO, human SNCA and SNCA/AEP mice (2–3 months old) with rotenone, 10 months earlier than appearance of any motor deficits in human SNCA transgenic mice.⁴² At the end of the neurotoxin treatment regimen, we found substantial TH neuronal loss in the SN and gut of SNCA/AEP WT mice but not in SNCA/AEP KO mice (Fig. 4e–g). In alignment with these findings, rotarod behavioral test demonstrated that rotenone elicited prominent motor dysfunction in SNCA/AEP WT but not SNCA/AEP KO mice (Fig. 4a). Therefore, these observations indicate that rotenone activates AEP that subsequently cleaves both α-Syn and Tau, leading to TH loss and motor impairments in PD pathogenesis.

Pathological α-Syn propagates along major CNS pathways to regions far beyond injection sites and reduces survival with a highly reproducible interval from injection to death in inoculated animals. Strikingly, inoculation with α-Syn fibrils assembled from recombinant human α-Syn induces identical consequences. Thus, a prion-like cascade in synucleinopathies whereby cell-cell transmission and propagation of misfolded α-Syn underlie the CNS spread of LBs/LNs.^{36,43} Remarkably, colonic-inoculated PFFs (α-Syn N103/Tau N368) propagate much more slowly in SNCA/AEP-null mice (12 days) than in SNCA/AEP WT mice (9 days) (Supplementary information, Fig. S6), suggesting that AEP participates in mediating the fibril transportation and spreading of α-Syn and Tau pathologies. These observations are alignment with our findings that PFF (α-Syn N103/Tau N368)-elicited p-S129 and AT8 signals are diminished in AEP^{-/-} neurons as compared with WT neurons (Supplementary information, Fig. S3). Conceivably, PFFs may penetrate into neurons and elicit endogenous AEP activation via triggering mitochondrial malfunction and oxidative stress, initiating a vicious cycle. Subsequently, active AEP might incur Tau and α-Syn truncation, promoting the fragment interaction and fibrillization, which may spread in a prion-like way. Interestingly, colonic inoculation of PFFs (α-Syn N103/Tau N368) initiates Tau pathologies in both LC and HC, in addition to NTS (Fig. 6). It has been reported that the NTS → nucleus paragigantocellularis (PGi) → LC → CA1 region of dorsal hippocampus pathway is important for consolidation of object recognition memory.⁴⁴ Moreover, neuronal loss in the LC of PD patients is likely to play an important role in PD-related disorders of posture and locomotion. Among PD patients without concurrent AD, the presence of dementia is associated with significantly lower LC neuronal counts.^{45,46} Hence, it is not surprising that we also observe the cognitive deficits in MWM and novel object recognition assays, and other PDD-like symptoms after colonic inoculation of PFFs (α-Syn N103/Tau N368). In addition to Tau pathologies in NTS/LC/HC pathway, colonic PFFs (α-Syn N103/Tau N368) also transmitted α-Syn pathology to DMV/SN/Striatum. Consequently, they stimulated TH-positive dopaminergic neuronal

loss in both SN and striatum, resulting in motor disorders in SNCA/AEP WT mice (Fig. 6). Interestingly, most recently, it has been reported that a nigro-vagal pathway controls gastric motility in a rat Parkinsonism.⁴⁷ This finding, combined with our observations, strongly suggest the mutual crosstalk between SNpc and gut via vagus nerves during the prodromal stage. Tau N368 PFFs in the brainstem might propagate via NTS to LC then to HC, mediating cognitive functions and depressive behaviors, resemblance to the symptoms associated with Parkinsonism. Nonetheless, the DMV appears to play a more prominent role in the pathophysiology of PD. Previous studies demonstrate that both Tau and α-Syn pathologies spread to distant and synaptically connected regions.^{43,48} Tau displays different conformations in different tauopathies, and they possess various strains with different propagation and Prion-like properties. Moreover, the distinct strains in tauopathies reveal differential cellular and brain region predispositions.^{48,49} Furthermore, Tau strains can only be propagated in Tau P301S transgenic mice but not WT mice.⁴⁸ Therefore, in order to explore α-Syn N103/Tau N368 fibril spreading from the gut to the brain, we employed human SNCA transgenic mice. In addition, AEP only cleaves human but not mouse α-Syn at N103. Hence, we chose human SNCA transgenic mice but not WT mice to assess the PFF spreading. Imaginably, it will be interesting to investigate whether the toxic α-Syn N103/Tau N368 PFFs also spread to the brain and elicit PD pathologies in WT mice. It is worth noting that Tau N368 PFFs provoke α-Syn S129 phosphorylation and aggregation via cross-seeding, whereas α-Syn N103 PFFs barely induce Tau AT8 phosphorylation in neurons (Figs. 3 and 6). Nonetheless, we only found p-S129 in different stereotypic interconnected brain regions after intrastratal inoculation of PFFs (α-Syn N103/Tau N368), but failed to observe Tau phosphorylation in other neural circuitry connected regions except the injected striatum in WT mice. Therefore, these findings support that Tau pathology transmission *in vivo* requires either α-Syn or Tau overexpression in SNCA or Tau P301S transgenic mice. Recently, it has been reported that α-Syn fibrils bind to LAG3 receptor, and the complex is internalized via endocytosis and transmit α-Syn pathology between neurons.⁵⁰ Moreover, α-Syn fibrils trigger neuronal degeneration via activating PARP1 in the parthanatos pathway.⁵¹ Conceivably, α-Syn N103 fibrils may display even stronger binding affinity toward LAG3 receptor and provoke dopaminergic neuronal loss via activating PARP1. Exploring whether inactivation of either LAG3 or PARP1 antagonizes α-Syn N103 neurotoxicity will provide novel mechanistic insight into its pathological role in PD. Together, our novel observations demonstrate that AEP-cleaved Tau and α-Syn form the fibrils in the colon that travel along the vagus nerve from the gut to the brain, and induce dopaminergic neuronal loss in SN, initiating PD pathogenesis and various motor and non-motor dysfunctions. Clearly, δ-secretase is a novel disease-modifying drug target for treating PD.

MATERIALS AND METHODS

Mice, primary cultured rat neurons, cell lines and human tissue samples

SNCA-null mice (B6;129X1-Sncatm1Ros1, stock# 003692) and human SNCA-overexpressing mice (B6.Cg-Tg(SNCA)OVX37Rwm Sncatm1Ros1/J, stock# 023837) on pure genetic background were backcrossed. Animal care and handling was performed according to NIH animal care guidelines and Emory Medical School guidelines. The protocol was reviewed and approved by the Emory Institutional Animal Care and Use Committee. Primary rat cortical and dopaminergic neurons were cultured as previously described.³⁰ All rats were purchased from the Jackson Laboratory. The protocol was reviewed and approved by the Emory Institutional Animal Care and Use Committee. SH-SY5Y cells were cultured in DMEM/F12 added with 10% FBS and penicillin (100

units/mL)-streptomycin (100 µg/mL) (all from Hyclone). Cells were incubated at 37 °C in a humidified atmosphere of 5% CO₂. Post-mortem brain samples were dissected from frozen brains of AD and aged-matched non-demented controls from the Emory Alzheimer's Disease Research Center. The study was approved by the Biospecimen Committee. PD was diagnosed according to the criteria of the Consortium to Establish a Registry for PD and the National Institute on Aging. Informed consent was obtained from the subjects. AEP antibody 6E3 was described previously.³¹ AT8 (MN1020), AT100 (MN1060), GST (MA4-004-HRP), c-Myc (9E10) and tubulin (236-10501) antibodies were purchased from Thermo Fisher. AEP and Tau N368³⁰ antibodies were generated in our laboratory. Recombinant human Legumain/AEP was purchased from Novoprotein (C-371). Antibodies used in the study are listed in Supplementary information, Table S1.

Cell viability

Cell viability was measured colorimetrically using the Cell-Titer Blue (CTB, Promega, Madison, WI, USA) fluorescence-based assay. Cells were plated at a density of 1000 cells/well in 96-well plates (BD Biosciences, San Diego, CA, USA). Six different PFFs were directly introduced to each well after DIV10 and then incubated for an additional 4 days. After incubation, 30 µL CTB reagent was added to each well and incubated at 37 °C and 5% CO₂ for 2.5–5 h. Fluorescence of the resorufin product was measured on a FluoDia T70 fluorescence plate reader (Photon Technology International, Birmingham, NJ, USA). Wells that included vehicle but not protein served as the negative control (0% toxic), and wells containing 10% DMSO were the positive control (100% toxic). Percent toxicity was calculated using the following equation:

$$\% \text{ Toxicity} = 100 - [100(\{S\} - \{P\}/\{N\} - \{P\})]$$

Each independent variable is the average of 3 plate replicates from the negative control ($\{N\}$), positive control ($\{P\}$), and samples ($\{S\}$). Results presented for viability experiments are an average of 3 experiments conducted independently on different days. Error bars represent the standard error of the mean (SEM).

Purification of human α-Syn FL and α-Syn N103 or GST-Tau FL and Tau N368

α-Syn FL and α-Syn N103 cDNAs were subcloned into *Nde*I and *Hind*III restriction sites of the bacterial expression vector pRK172, and the proteins were expressed in *Escherichia coli* BL21 (DE3). Tau cDNAs were subcloned into the *Not*I and *Sal*I restriction sites of the bacterial expression vector GST, and the respective proteins were expressed in BL21 (DE3). Bacterial pellets were resuspended in high-salt buffer (0.75 M NaCl, 50 mM Tris, pH 7.4, 1 mM EDTA) containing a mixture of fresh protease inhibitors, sonicated at 25% power for 3 min in the ice (3 times), and centrifuged at 70,000 × g for 30 min. The supernatants were applied onto a Glutathione Sepharose column (GE Healthcare) and purified by GST tag. We used thrombin to remove GST tag. One unit cleaves theoretical 100 µg protein in 16 h at 22 °C in PBS buffer (150 mM NaCl, 2.7 mM KCl, 10 mM Na₂HPO₄, 1.8 mM KH₂PO₄, pH 7.4). After that, 4 different proteins were dialyzed in FPLC buffer (50 mM NaCl, 50 mM Tris-HCl, pH 7.4) overnight at 8 °C to change the buffer salt concentration. Proteins were filtered through a 0.22 µm syringe filter and injected into the FPLC machine (Superdex 200 column; GE Healthcare). The fractions were assayed for the presence of the α-Syn FL and α-Syn N103, Tau FL (4R2N) and Tau N368 proteins by SDS-PAGE followed by Coomassie Blue staining. Protein concentration was determined by the Bradford protein assay (Pierce) using bovine serum albumin (BSA) as a standard.

Determination of endotoxins

LAL assay is widely used to detect and quantitate endotoxins originating from gram-negative bacteria. In our experiments, a

chromogenic LAL test (ToxicSensor Chromogenic LAL Endotoxin Assay Kit, Genscript, Piscataway, NJ, USA) was used to determine the amount of endotoxins. The concentrations of endotoxin were calculated according to the manufacturer's guidelines with the formula $0.2618 \times X - 0.0012$ (where X is the absorbance at 545 nm of each sample). We tested whether the protein endotoxin levels were decreased after elution from Pierce High Capacity Endotoxin Removal Spin Columns. Endotoxin levels were reduced to a final concentration of < 5 EU/mL after spin column extraction. This final EU concentration would not affect cytokine and cellular toxin levels.

Generation of 6 different PFFs

Fibrils were prepared in reactions (500 µL per tube) containing 3 mg/mL of α-Syn FL and α-Syn N103, Tau FL (4R2N) and Tau N368 protein monomers in PFF reaction buffer (50 mM Tris-HCl, pH 7.4, 50 mM NaCl). The proteins were incubated for several days at 37 °C, with orbital shaking at 300 rpm until samples appeared cloudy. Usually, the reactions were subjected to 7–9 days shaking for the PFF generation. PFFs were validated by Th-T in vitro assay.

Cellular PFF uptake by biotin signal analysis

Biotin was used to monitor PFF uptake by mouse midbrain neurons. Biotin labeling is a process of covalently attaching biotin to a protein. For neuron uptake experiments, neurons were plated in DMEM/F12 medium in 6 wells coated with poly-D-lysine and laminin and cultured for DIV10 prior to measurements. Control wells contained the same volume of PBS with neurons, for cell toxicity and biotin fluorescence. Six different biotinylated PFFs were added to the wells at the start of the experiments, and the biotin fluorescence curves were taken in the neurons, at a height of 100 µm from the bottom to surface of the wells. The curves were collected at regular intervals, over a period ranging from 2 to 24 h, and each curve was integrated for 30 s and repeated 5 times.

AEP activity assay

Tissue homogenates or cell lysates (10 µg) were incubated in 200 µL reaction buffer (20 mM citric acid, 60 mM Na₂HPO₄, 1 mM EDTA, 0.1% CHAPS and 1 mM DTT, pH 5.5) containing 20 µM AEP substrate Z-Ala-Ala-Asn-AMC (Bachem). AMC released by substrate cleavage was quantified by measuring at 460 nm in a fluorescence plate reader at 37 °C in kinetic mode.

Th-T assay

Th-T stock solution was prepared by adding 8 mg Th-T to 10 mL PBS and filtering through a 0.2 µm syringe filter (Sigma-Aldrich, Cat# T3516). The stock solution was diluted into the phosphate buffer (1 mL Th-T stock to 50 mL buffer) to generate the working solution. Th-T working solution with PFFs (7 µM) was excited at 440 nm and emitted at 482 nm to measure the fluorescence intensity on the plate reader (Bioteck, #251639, Vermont, USA). For the PFF seeding test, different ratios of mixed PFFs/monomer (1:10, 1:35, 1:70 and 1:100) were incubated on the orbital shaker at 37 °C for 1 h. The fluorescence values onto plate reader were recorded.

Biacore X100

The carboxylated dextran matrix of the sensor chip was activated by the injection of 60 µL of solution containing 0.2 M N-ethyl-N'-(3-dimethylaminopropyl) carbodiimide and 0.05 M N-hydroxysuccinimide in water. We used the activation buffers from the kit, EDC + NHS. Immobilization step running time was 180 s. Purified α-Syn or α-Syn N103 proteins were immobilized at a concentration of 50 µg/mL in 10 mM sodium acetate (pH 4.0). 50 mM NaOH was employed for regeneration in 75 µL, maximum volume of deionized water and running buffer (HEPES + EDTA + P20) (BIAcore, GE Healthcare). The remaining binding sites were blocked with 1 M ethanolamine (pH 8.5). Screening of purified proteins (Tau FL and Tau N368) for binding to α-Syn FL and α-Syn N103 was performed by injecting aliquots (120 µL) of samples

(~100 µg protein/mL) onto the derivatized sensor chip. CM5 chip was used for regeneration step. Regeneration of the sensor chip after each analysis cycle was performed by injecting 20 µL of 1.5 M glycine/HCl buffer (pH 3.5) and 6 M guanidinium HCl (pH 5.5).

Immunofluorescence staining

AEP WT, AEP KO neurons, mouse colon and brain SN tissues were fixed with 4% paraformaldehyde/4% sucrose (primary neurons), 4% paraformaldehyde (colon tissue) and 4% paraformaldehyde/30% sucrose (brain SN) in PBS followed by permeabilization with PBS-T (50 mM Tris-HCl, pH 7.4, 150 mM NaCl, 3% BSA, 0.1% Triton X-100) solution. To analyze the pathological progression of PD, we used various antibodies such as α-Syn pS129 (Santa Cruz, Cat# SC69977); α-Syn N103 (1:1000; Ye Lab); α-Syn N103-biotin (1:1000; Ye Lab); Tau AT8 (1:1000; Thermo Fisher, Cat# MN1020); Tau N368 (1:2000; Ye lab); AEP 6E3 (1:1000; Colin Watts Lab); Tyrosine Hydroxylase (1:1000; Sigma, Cat# T2928 or Thermo Fisher, Cat# AB152). Neurons, colon and brain SN (mouse) tissues were incubated with primary antibodies (α-Syn pS129 (1:500) and Tau AT8 (1:1000)). After three times washing in PBS, the sections were incubated with the fluor-conjugated secondary antibody (Streptavidin, Alexa Fluor 488 conjugate (1:3000); Thermo Fisher, Cat# S11227) for 2 h at room temperature (RT). After 4', 6-diamidino-2-phenylindole (DAPI) staining for 5 min, the slides were washed three times in PBS and covered with a glass using mounting solution.

PD patients' gut biopsy and immunofluorescent staining

The included subjects were recruited from patients (55–70 years old) suffering from PD and constipation ($n = 4$). PD was diagnosed according to MDS clinical diagnostic criteria. Constipation was assessed using Patient Assessment of Constipation symptom (PAC-SYM). The excluded subjects were those with Parkinson's syndrome, colon disease and other digestive diseases. The age-matched subjects without PD and constipation were selected as control group ($n = 4$). Electronic colonoscopy and mucosal biopsy examination were performed in all subjects. The intestine tissue specimens of 0.8 cm thickness were cut about 5 cm away from the valves of colon, containing mucous layer and submucosa. The samples were placed in 95% alcohol after cutting, and embedded in paraffin for further immunofluorescence. The paraffin-embedded tissues were sectioned at thickness of 4 µm. Intestine sections were mounted on glass slides, deparaffinized in xylene, dehydrated in graded ethanol solutions, baked in basic antigen retrieval buffer (pH 6.0), and washed with phosphate buffer (pH 7.4). The sections were blocked with 3% BSA for 50 min at RT, and incubated with diluted primary antibody in a humidified chamber at 4 °C overnight. After primary antibody incubation, all sections were washed with phosphate buffer (pH 7.4), and subsequently incubated with an appropriately diluted Cyanine 3- or Alexa 488-coupled secondary antibody in dark for 50 min followed by nucleus dyeing by DAPI for 10 min. Images were acquired using laser confocal microscopy and analyzed using Image-Pro Plus software by an independent experimenter blinded to the sections ($n = 4$ sections for counting).

Stereological cell quantification

Unbiased stereological cell counting was performed using the Stereo Investigator software (MBF Bioscience, Williston, VT, USA). All SN sections of 30 µm at every 6th section were stained with TH antibody. They were analyzed under the randomly placed counting frames (50 × 50 µm) on a counting grid (120 × 120 µm). Optical disector of 22 µm with 2 µm upper and lower guard zones was used. The SN boundaries were outlined under magnification of the 5× objective lens and cells were counted with the 40× objective lens using an Olympus BX53 microscope. The total number of neurons in the SN was estimated using the optical fractionator method. TH-positive axon terminal in striatum was estimated using fluorescence intensity by Image J software. For

quantification of positive cells, stained color was selected and the proper threshold was set for the binarization of the selected color image. The total number of immunoreactive neurons was analyzed using the same threshold (Image J). The conditions of the analysis were blinded to the investigator.

Immunohistochemistry

Mouse brain sections sliced by cryotome or paraffin-embedded human brain sections were treated with 0.3% H₂O₂ for 10 min. Sections were washed three times in PBS and blocked in 1% BSA, 0.3% Triton X-100, for 30 min, followed by overnight incubation with TH antibody (1:1000), anti-α-Syn or N103 antibody (1:500) at 4 °C. The signal was developed using Histostain-SP kit (Invitrogen).

Transmission electron microscopy (TEM)

Electron microscopy images were produced from α-Syn FL, α-Syn N103, Tau FL, Tau N368, α-Syn FL + Tau FL and α-Syn N103 + Tau N368 after PFFs were generated. The samples (5 µL) were deposited on Formvar-coated 400 mesh copper grids, fixed with 0.5% glutaraldehyde, negative stained with 2% uranyl acetate (Sigma-Aldrich, Germany) and screened by CM-10 TEM.

X-ray diffraction

Dried stock samples were prepared for X-ray fiber diffraction by vortexing α-Syn FL, α-Syn N103, Tau FL, Tau N68, α-Syn FL + Tau FL and N103 + N368 PFFs for 30 min at RT. The PFFs were lyophilized for 3 days using a freeze-drying machine for X-ray diffraction. The sample-to-detector distance was 300 mm, with an exposure time of 30 s. Diffraction patterns were converted to Tiff files using the program fit-2d (Hammersley/ESRF) and radially integrated to generate one-dimensional scattering patterns using Matlab code. The X-ray diffraction patterns for dried fibrils were radially integrated in either the equatorial or meridional direction using a 30-degree sector in the azimuthal direction on either side of the anionic reflection. The position of maximum intensity was used to determine the position of anionic reflections and the difference in position of either side of the pattern was used to assess the error in the position of the reflection. The variation in X-ray intensity for the reflections at α-Syn FL PFFs 4.39 Å, 4.48 Å, 4.87 Å and 15.71 Å; α-Syn N103 PFFs 4.51 Å, 4.91 Å, 5.41 Å and 15.61 Å; Tau FL PFFs 4.55 Å, 11.11 Å, 16.45 Å, 3.11 Å and 20.11 Å; Tau N368 PFFs 2.14 Å, 4.29 Å, 5.11 Å and 7.21 Å; α-Syn FL + Tau FL PFFs 3.12 Å, 4.34 Å, 4.94 Å and 14.12 Å; α-Syn N103 + Tau N368 PFFs 1.64 Å, 4.21 Å, 6.94 Å and 7.33 Å (fibril reaction buffer: 50 mM Tris-HCl, pH 7.0, 50 mM NaCl). We also determined X-ray intensity using the same Matlab code. A calibrant of high density polyethylene (HDPE) was used to determine the position of the beam sample-to-detector distance and pixel size.

Oral gavage of rotenone

Mice were treated with 0.1 mL/25 g of vehicle containing 1% methylcellulose (Sigma, Cat# M0512) and 1.25% chloroform (Sigma, Cat# 2432) or a solution containing 0.625 mg/mL of rotenone (ULTRA Scientific, Cat# PST-890) with 1% methylcellulose and 1.25% chloroform. We prepared rotenone solution by dissolving rotenone in chloroform and then diluting into 1% methylcellulose solution while mixing vigorously. Rotenone or vehicle control was orally administered with a 1.2 × 60 mm gavage (Unimed, Switzerland) once a day for 5 days/week, consecutively for 3 months.

Measurement of rotenone levels in mouse colon and brain

Colon and brain samples were obtained by ultracentrifugation at 80,000 rpm for 30 min, and rotenone was extracted with 300 µL ethyl acetate-DCM (1:1 ratio) three times on a vortexer. After centrifugation at 5000 rpm for 5 min, the organic phase was transferred to another clean test tube and rapidly eliminated by evaporation at RT under N₂ flow. The residue was dissolved in 100 µL methanol, and 10 µL was analyzed by high performance

liquid chromatography (HPLC) following experimental condition: 717 autosampler, model 1525 binary pump and model 2996 photodiode array detector (Waters), Waters Spherisorb ODS2 column (4.6 × 150 mm, 3 µM, Waters) with Spherisorb ODS2 Guard Cartridge (80 Å, 5 µm, 4.6 mm × 10 mm), flow rate of 1.5 mL/min, run time of 35 min.

Stereotaxic injection

PFFs of α-Syn, Tau, α-Syn N103, Tau N368, FL combination, or fragment combination were sonicated as indicated in previous literature,⁵² and injected into the striatum of mice. Three months old mice of each group were anesthetized with isoflurane (Piramal Healthcare). Meloxicam (2 mg/kg) was injected subcutaneously for analgesics (Loxicom, Norbrook). Unilateral intracerebral injection of PFFs was performed stereotactically at the following coordinates: anteroposterior (AP) –3.1 mm and mediolateral (ML) –1.2 mm relative to bregma, and dorsoventral (DV) –4.3 mm from the dural surface. 2 µL of PFF (3 µg) was injected into each site using 10 µL Hamilton syringe with a fixed needle at a rate of 0.25 µL/min. The needle remained in place for 5 min after the PFF solution was completely injected. The needle was removed slowly (over 2 min). The mice were placed on heating pad until it began to recover from the anesthesia.

Mouse colonic injection

To make the colonic injection of the PFF solutions (3 µg), a high-resolution miniaturized colonoscope system (Coloview Veterinary Endoscope, Karl Storz) was used.⁵³ In short, this system consisted of a miniature rigid endoscope (1.9 mm outer diameter), a xenon light source, a triple-chip high-resolution charge-coupled device camera, and an operating sheath with instrument channels (all from Karl Storz). The endoscope with outer operating sheath was inserted into the mid-descending colon and the injection was performed with the aid of a custom-made device comprising a needle (OD: 0.2 mm) connected to a small tube fitted with a syringe. Colonic injection procedures were viewed with high-resolution (1024 × 768 pixels) live video on a flat-panel color monitor.

Vagotomy and vagus nerve isolation

The sonicated PFFs were injected into colon and vagotomy was performed 2 days after colonic injection. Colon-injected mice were anesthetized with isoflurane and Meloxicam (2 mg/kg) was injected subcutaneously for analgesics. After cervical midline incision, vagus nerve around common carotid artery was isolated and cut on one side. Mice were sacrificed 7 days after vagotomy, and the brainstem regions for vagus nerve were sliced. To isolate vagus nerve, we opened the mouse tracheal region, and identified the trachea, carotid artery and the masticatory muscles, after mice were euthanized. Then, we removed the trachea to allow the access to the carotid and the adhering vague nerve and cleanly isolated the carotid from the surrounding tissues, without cutting the vagus nerve, which were immediately fixed in 4% paraformaldehyde.

Gastrointestinal motility assays

Stool water content was measured in mice as described previously.⁵⁴ Red carmine dye test was used to measure the total GI tract transit time.⁵⁵

Behavioral tests

Loss of motor function due to dopaminergic neurodegeneration was tested 3 months following the PFF injection. Behavioral tests included the rotarod test, cylinder test, tail suspension test, object recognition test, and water maze test.

Rotarod test

Mice were trained for 3 days using the Rotarod (San Diego Instruments) at a slow rotational speed (5 rpm) for a maximum of 10 min. The rotational speed and latency to fall from the

accelerating Rotarod were recorded, after three test trials on the test day. The rotational speed of Rotarod was modulated from 0 rpm to a maximum of 40 rpm. It was gradually increased during the trial at a rate of 0.1 rpm/s.

Grid performance test

The mice were placed on a horizontal grid. The grid was inverted, and thus the mice were hanging upside down by their paws. Animals were videotaped for up to 60 s, and then a 10 s segment was scored for forepaw step distance as defined by the number of grids transversed with each step.

Tail suspension test

Tape was adhered to the tails of mice, after the camera was placed in position. Mice were suspended by placing the free end of the tape on the suspension bar. Their behaviors were recorded for 6 min and the immobilized time was analyzed.

Novel object recognition test

For habituation, mice were placed in open field and allowed to freely explore for 5 min. On the next day, two different objects were put in opposite corners of the open field and mice were placed in the middle of the open field to explore for 10 min. For the test, one of the same object used during training was replaced with one novel object in opposite corner. Mice were placed in the middle of the field and allowed for free exploration for 10 min. Time spent in exploring the novel object was analyzed and the discrimination index was calculated.

Water maze test

Mice were trained in a round, water-filled tub (52 inches in diameter) in an environment rich in extra maze cues. Each mouse was given 4 trials/day for 5 consecutive days with a 15-min inter-trial interval. Mice were manually guided to the platform, when they did not find it in the given time (60 s). Following the 5 days of task acquisition, a probe trial was presented during which the platform was removed and the percentage of time spent in the quadrant which previously contained the escape platform during task acquisition was measured over 60 s. All trials were analyzed for latency and swim speed by means of MazeScan (Clever Sys, Inc.).

Quantification and statistical analysis

All data are expressed as means ± SEM from three or more independent experiments, and the level of significance between two groups was assessed with Student's *t*-test. For more than two groups, two-way ANOVA followed by LSD post hoc test was applied. A *P* value < 0.05 was considered to be statistically significant. Effect size of samples was determined by Power analysis (Biostat).

ACKNOWLEDGEMENTS

We thank ADRC at Emory University for human AD patients and healthy control samples. This work was supported by grants from NIH RF1 (AG051538) to K.Y. HPLC analysis was supported in part by the Emory HPLC Bioanalytical Core (EHBC), which was supported by the Department of Pharmacology, Emory University School of Medicine and the Georgia Clinical & Translational Science Alliance of the National Institutes of Health under Award Number UL1TR002378. The content is solely the responsibility of the authors and does not necessarily reflect the official views of the National Institutes of Health.

AUTHOR CONTRIBUTIONS

K.Y. and X.C. conceived the project, designed the experiments, and wrote the manuscript. E.H.A. and S.S.K. designed and performed most of the experiments. G.C. and Z.Z. performed and helped with immunohistochemistry experiments. X.L. prepared primary neurons; B.C. and A.M.A. assisted with colonoscopy experiments. A.S.N. and X.C. assisted with data analysis and interpretation and critically read the manuscript.

ADDITIONAL INFORMATION

Supplementary information accompanies this paper at <https://doi.org/10.1038/s41422-019-0241-9>.

Competing interests: The authors declare no competing interests.

REFERENCES

- Savitt, J. M., Dawson, V. L. & Dawson, T. M. Diagnosis and treatment of Parkinson disease: molecules to medicine. *J. Clin. Invest.* **116**, 1744–1754 (2006).
- Olanow, C. W. & Brundin, P. Parkinson's disease and alpha synuclein: is Parkinson's disease a prion-like disorder? *Mov. Disord.* **28**, 31–40 (2013).
- Hirai, Y., Fujita, S. C., Iwatsubo, T. & Hasegawa, M. Phosphorylated alpha-synuclein in normal mouse brain. *FEBS Lett.* **572**, 227–232 (2004).
- Kruger, R. et al. Ala30Pro mutation in the gene encoding alpha-synuclein in Parkinson's disease. *Nat. Genet.* **18**, 106–108 (1998).
- Polymeropoulos, M. H. et al. Mutation in the alpha-synuclein gene identified in families with Parkinson's disease. *Science* **276**, 2045–2047 (1997).
- Zarranz, J. J. et al. The new mutation, E46K, of alpha-synuclein causes Parkinson and Lewy body dementia. *Ann. Neurol.* **55**, 164–173 (2004).
- Simon-Sánchez, J. et al. Genome-wide association study reveals genetic risk underlying Parkinson's disease. *Nat. Genet.* **41**, 1308–1312 (2009).
- Yasuda, T., Nakata, Y., Choong, C. J. & Mochizuki, H. Neurodegenerative changes initiated by presynaptic dysfunction. *Transl. Neurodegener.* **2**, 16 (2013).
- Arima, K. et al. Cellular co-localization of phosphorylated tau- and NACP/alpha-synuclein-epitopes in Lewy bodies in sporadic Parkinson's disease and in dementia with Lewy bodies. *Brain Res.* **843**, 53–61 (1999).
- Ishizawa, T., Mattila, P., Davies, P., Wang, D. & Dickson, D. W. Colocalization of tau and alpha-synuclein epitopes in Lewy bodies. *J. Neuropathol. Exp. Neurol.* **62**, 389–397 (2003).
- Edwards, T. L. et al. Genome-wide association study confirms SNPs in SNCA and the MAPT region as common risk factors for Parkinson disease. *Ann. Hum. Genet.* **74**, 97–109 (2010).
- Jensen, P. H. et al. alpha-synuclein binds to Tau and stimulates the protein kinase A-catalyzed tau phosphorylation of serine residues 262 and 356. *J. Biol. Chem.* **274**, 25481–25489 (1999).
- Giasson, B. I. et al. Initiation and synergistic fibrillization of tau and alpha-synuclein. *Science* **300**, 636–640 (2003).
- Waxman, E. A. & Giasson, B. I. Induction of intracellular tau aggregation is promoted by alpha-synuclein seeds and provides novel insights into the hyperphosphorylation of tau. *J. Neurosci.* **31**, 7604–7618 (2011).
- Guo, J. L. et al. Distinct alpha-synuclein strains differentially promote tau inclusions in neurons. *Cell* **154**, 103–117 (2013).
- Roy, B. & Jackson, G. R. Interactions between Tau and alpha-synuclein augment neurotoxicity in a *Drosophila* model of Parkinson's disease. *Hum. Mol. Genet.* **23**, 3008–3023 (2014).
- Hatcher, J. M., Pennell, K. D. & Miller, G. W. Parkinson's disease and pesticides: a toxicological perspective. *Trends Pharm. Sci.* **29**, 322–329 (2008).
- Lummen, P. Complex I inhibitors as insecticides and acaricides. *Biochim Biophys. Acta* **1364**, 287–296 (1998).
- Betarbet, R. et al. Chronic systemic pesticide exposure reproduces features of Parkinson's disease. *Nat. Neurosci.* **3**, 1301–1306 (2000).
- Cannon, J. R. et al. A highly reproducible rotenone model of Parkinson's disease. *Neurobiol. Dis.* **34**, 279–290 (2009).
- Talpade, D. J., Greene, J. G., Higgins, D. S. Jr. & Greenamyre, J. T. In vivo labeling of mitochondrial complex I (NADH:ubiquinone oxidoreductase) in rat brain using [(3)H]dihydrotetradecanoate. *J. Neurochem.* **75**, 2611–2621 (2000).
- Sherer, T. B. et al. An in vitro model of Parkinson's disease: linking mitochondrial impairment to altered alpha-synuclein metabolism and oxidative damage. *J. Neurosci.* **22**, 7006–7015 (2002).
- Betarbet, R. et al. Intersecting pathways to neurodegeneration in Parkinson's disease: effects of the pesticide rotenone on DJ-1, alpha-synuclein, and the ubiquitin-proteasome system. *Neurobiol. Dis.* **22**, 404–420 (2006).
- Wang, X. F., Li, S., Chou, A. P. & Bronstein, J. M. Inhibitory effects of pesticides on proteasome activity: implication in Parkinson's disease. *Neurobiol. Dis.* **23**, 198–205 (2006).
- Drolet, R. E., Cannon, J. R., Montero, L. & Greenamyre, J. T. Chronic rotenone exposure reproduces Parkinson's disease gastrointestinal neuropathology. *Neurobiol. Dis.* **36**, 96–102 (2009).
- Greene, J. G., Noorian, A. R. & Srinivasan, S. Delayed gastric emptying and enteric nervous system dysfunction in the rotenone model of Parkinson's disease. *Exp. Neurol.* **218**, 154–161 (2009).
- Holmqvist, S. et al. Direct evidence of Parkinson pathology spread from the gastrointestinal tract to the brain in rats. *Acta Neuropathol.* **128**, 805–820 (2014).
- Pan-Montojo, F. et al. Environmental toxins trigger PD-like progression via increased alpha-synuclein release from enteric neurons in mice. *Sci. Rep.* **2**, 898 (2012).
- Li, D. N., Matthews, S. P., Antoniou, A. N., Mazzeo, D. & Watts, C. Multistep autoactivation of asparaginyl endopeptidase in vitro and in vivo. *J. Biol. Chem.* **278**, 38980–38990 (2003).
- Zhang, Z. et al. Cleavage of tau by asparagine endopeptidase mediates the neurofibrillary pathology in Alzheimer's disease. *Nat. Med.* **20**, 1254–1262 (2014).
- Zhang, Z. et al. Delta-secretase cleaves amyloid precursor protein and regulates the pathogenesis in Alzheimer's disease. *Nat. Commun.* **6**, 8762 (2015).
- Zhang, Z. et al. Inhibition of delta-secretase improves cognitive functions in mouse models of Alzheimer's disease. *Nat. Commun.* **8**, 14740 (2017).
- Zhang, Z. et al. Asparagine endopeptidase cleaves alpha-synuclein and mediates pathologic activities in Parkinson's disease. *Nat. Struct. Mol. Biol.* **24**, 632–642 (2017).
- Braak, H., Ghebremedhin, E., Rub, U., Bratzke, H. & Del Tredici, K. Stages in the development of Parkinson's disease-related pathology. *Cell Tissue Res.* **318**, 121–134 (2004).
- Volpicelli-Daley, L. A. et al. Exogenous alpha-synuclein fibrils induce Lewy body pathology leading to synaptic dysfunction and neuron death. *Neuron* **72**, 57–71 (2011).
- Luk, K. C. et al. Pathological alpha-synuclein transmission initiates Parkinson-like neurodegeneration in nontransgenic mice. *Science* **338**, 949–953 (2012).
- McDowell, K. & Chesselet, M. F. Animal models of the non-motor features of Parkinson's disease. *Neurobiol. Dis.* **46**, 597–606 (2012).
- Kaur, H., Chauhan, S. & Sandhir, R. Protective effect of lycopene on oxidative stress and cognitive decline in rotenone induced model of Parkinson's disease. *Neurochem. Res.* **36**, 1435–1443 (2011).
- Santiago, R. M. et al. Depressive-like behaviors alterations induced by intranigral MPTP, 6-OHDA, LPS and rotenone models of Parkinson's disease are predominantly associated with serotonin and dopamine. *Prog. Neuropsychopharmacol. Biol. Psychiatry* **34**, 1104–1114 (2010).
- Braak, H. et al. Staging of brain pathology related to sporadic Parkinson's disease. *Neurobiol. Aging* **24**, 197–211 (2003).
- Braak, H., de Vos, R. A., Bohl, J. & Del Tredici, K. Gastric alpha-synuclein immunoreactive inclusions in Meissner's and Auerbach's plexuses in cases staged for Parkinson's disease-related brain pathology. *Neurosci. Lett.* **396**, 67–72 (2006).
- Janezic, S. et al. Deficits in dopaminergic transmission precede neuron loss and dysfunction in a new Parkinson model. *Proc. Natl. Acad. Sci. USA* **110**, E4016–E4025 (2013).
- Luk, K. C. et al. Intracerebral inoculation of pathological alpha-synuclein initiates a rapidly progressive neurodegenerative alpha-synucleinopathy in mice. *J. Exp. Med.* **209**, 975–986 (2012).
- Mello-Carpes, P. B. & Izquierdo, I. The Nucleus of the Solitary Tract → Nucleus Paragigantocellularis → Locus Coeruleus → CA1 region of dorsal hippocampus pathway is important for consolidation of object recognition memory. *Neurobiol. Learn. Mem.* **100**, 56–63 (2013).
- Zweig, R. M., Cardillo, J. E., Cohen, M., Giere, S. & Hedreen, J. C. The locus ceruleus and dementia in Parkinson's disease. *Neurology* **43**, 986–991 (1993).
- Jellinger, K. A. Pathology of Parkinson's disease. Changes other than the nigrostriatal pathway. *Mol. Chem. Neuropathol.* **14**, 153–197 (1991).
- Anselmi, L., Toti, L., Bove, C., Hampton, J. & Travagli, R. A. A Nigro-Vagal pathway controls gastric motility and is affected in a rat model of Parkinsonism. *Gastroenterology* **153**, 1581–1593 (2017).
- Sanders, D. W. et al. Distinct tau prion strains propagate in cells and mice and define different tauopathies. *Neuron* **82**, 1271–1288 (2014).
- Hyman, B. T. Tau propagation, different tau phenotypes, and prion-like properties of tau. *Neuron* **82**, 1189–1190 (2014).
- Mao, X. et al. Pathological alpha-synuclein transmission initiated by binding lymphocyte-activation gene 3. *Science* **353**, aah3374 (2016).
- Kam, T. I. et al. Poly(ADP-ribose) drives pathologic alpha-synuclein neurodegeneration in Parkinson's disease. *Science* **362**, eaat8407 (2018).
- Tarutani, A. et al. The effect of fragmented pathogenic alpha-synuclein seeds on prion-like propagation. *J. Biol. Chem.* **291**, 18675–18688 (2016).
- Alam, A. et al. The microenvironment of injured murine gut elicits a local pro-restitutive microbiota. *Nat. Microbiol.* **1**, 15021 (2016).
- Chandrasekharan, B. P. et al. Adenosine 2B receptors (A2BAR) on enteric neurons regulate murine distal colonic motility. *FASEB J.* **23**, 2727–2734 (2009).
- Li, Z. et al. Essential roles of enteric neuronal serotonin in gastrointestinal motility and the development/survival of enteric dopaminergic neurons. *J. Neurosci.* **31**, 8998–9009 (2011).